User-Constrained Algorithms for Aggregate Residential Demand Response Programs with Limited Feedback.

by

Adam Charles Gray
B.Eng., University of Victoria, 2011

A Thesis Submitted in Partial Fulfillment of the
Requirements for the Degree of

Master of Applied Science

in the Department of Mechanical Engineering

User-Constrained Algorithms for Aggregate Residential Demand Response Programs with Limited Feedback.

by

Adam Charles Gray
B.Eng., University of Victoria, 2011

Supervisory Committee

Dr. Curran Crawford, (Department of Mechanical Engineering)
Supervisor

Dr. Ned Djilali, (Department of Mechanical Engineering)
Departmental Member

Abstract

Supervisory Committee

Dr. Curran Crawford, (Department of Mechanical Engineering)

Supervisor

Dr. Ned Djilali, (Department of Mechanical Engineering)

Departmental Member

This thesis presents novel algorithms and a revised modeling framework to evaluate residential aggregate electrical demand response performance under scenarios with limited device-state feedback. These algorithms permit the provision of balancing reserves, or the smoothing of variable renewable energy generation, via an externally supplied target trajectory. The responsive load populations utilized were home heat pumps and deferred electric vehicle charging. As fewer devices in a responsive population report their state information, the error of the demand response program increases moderately but remains below 8%. The associated error of the demand response program is minimized with responsive load populations of approximately 4500 devices; the available capacity of the demand response system scales proportionally with population size. The results indicate that demand response programs with limited device-state feedback may provide a viable option to reduce overall system costs and address privacy concerns of individuals wishing to participate in a demand response program.

Table of Contents

List of Tables

List of Figures

List of Abbreviations and Symbols

Abbreviations

AMSL	Above Mean Sea Level
BPA	Bonneville Power Authority
CAES	Compressed Air Energy Storage
CAISO	California Independent System Operator
CCGT	Closed Cycle Gas Turbine
CPEVS	Canadian Plug-in Electric Vehicle Survey
DR	Demand Response
EC	Electrochemical Capacitors
ETP	Equivalent Thermodynamic Parameter
EV	Electric Vehicle
GHG	Green House Gas
HVAC	Heating, Ventilation, and Air-Conditioning
LA	Load Aggregator
LC	Load Community
NREL	National Renewable Energy Laboratory
NRMSE	Normalized Root Mean Squared Error
O & M	Operations & Maintenance
OCGT	Open Cycle Gas Turbine
PCH	Programmable Communicating Hysteresis Controller
PEV	Plug-in Electric Vehicle
PHS	Pumped Hydro Storage
SMES	Superconducting Magnet Energy Storage
TCL	Thermostatically Controlled Load
TOU	Time of Use
VGM	Virtual Generator Model

Symbols

C_a	Indoor air thermal mass
C_m	Indoor building thermal mass
C_p	Wind turbine coefficient of performance
$C_{p,m}$	Turbine coefficient of performance at maximum wind speed
$C_{p,r}$	Turbine coefficient of performance at rated wind speed
D	Wind turbine blade diameter
e	Additional un-modeled system gains or losses (White noise term)
E	State of Charge of EV Battery
E_C	PEV Battery Capacity
$E_D^{(p)}$	Total energy dispatched from responsive load population p
E_S	Minimum required charging trajectory
i	Population index
k	Discrete time sampling index
m	Deadband location index
n	Operational State of Load
N_i	Number of loads in population
N_p	Number of responsive load communities
p	Responsive load type index
P	Current Device Power Consumption
P_0	Uncontrolled responsive load trajectory
P_{cap}	Total installed capacity in responsive load population
P_{cap}	Total power rating of aggregate responsive load population
P_h	Required electric power of heat pump at design temperature
P_{fan}	Required electric power of heat pump fan
P_m	Mechanical power imparted to wind turbine blades
P_{min}	Minimum responsive load population power output
P_{max}	Maximum responsive load population power output
$P_{r,i}$	Rated power of individual load
P_{rt}	Turbine rated power
P_T	Aggregate target trajectory for multiple responsive load communities

P_{wind}	Total power generated from wind turbine
P*	Target trajectory for individual responsive load population
ΔP^*	Target deviation from uncontrolled responsive load trajectory
S	Turbine gearbox number of stages
T	Sampling time interval (1 min)
T_S	Simulation Time Period
u	DR set point modulation control signal
u_{ci}	Turbine cut-in speed
u_{co}	Turbine cut-out speed
u_m	Turbine maximum wind speed
u_r	Turbine rated wind speed
u_s*	Target modulation control signal
u_w	Wind speed
$\dot{q}$	Total heat input to system
$\dot{q}_d$	Design heating rate of the heat pump
$\dot{q}_{fan}$	Heating power of heat pump fan operation
$\dot{q}_h$	Heating rate of heat pump
$\dot{\boldsymbol{q}}_{\boldsymbol{loss}}$	Rate of Heat transfer from house to environment
$\dot{\boldsymbol{q}}_{\boldsymbol{op}}$	Rate of heat transfer from heat pump to indoor air
R_{ao}	Building envelope heat transfer resistance
R_{ma}	Heat transfer resistance between building mass and air
$\mathbf{Z}$	Set of power state vectors
z_i	Individual load device power state vector
β	Wind turbine blade pitch angle
δ	Hysteresis control deadband width
ϵ_-	Device State-transition lower boundary
ϵ_+	Device State-transition upper boundary
ϵ	Device End-use state comparison
θ_a	Outdoor air temperature
θ_d	Heat pump system design temperature
θ_s	Thermostat temperature set point

θ_m	House thermal mass temperature
$\dot{\theta_a}$	Thermal trajectory of home indoor air
$\dot{\theta_m}$	Thermal trajectory of home thermal mass
Ω	ETP State-transformation matrix
Γ	ETP Input-transformation matrix
λ	Wind turbine tip-speed ratio
ρ	Air density
$\boldsymbol{\eta}$	Energy Conversion Efficiency
η_d	Heat pump efficiency at design temperature
η_e	Turbine electrical conversion efficiency
η_g	Turbine gearbox efficiency
Φ	Capacity factor of responsive load population
$\Phi_{limited}$	Capacity factor of reporting loads in responsive population
ϕ_0	Inactive power density distribution function
ϕ_1	Active power density distribution function
$\phi_{0,r}$	Inactive power density distribution function of reporting loads
$\phi_{1,r}$	Active power density distribution function of reporting loads
$\mathcal{F}^{(p)}$	Flexibility of responsive load population p
φ_{down}	Down-regulation under-utilization factor
φ_{up}	Up-regulation under-utilization factor
γ	Heat pump oversize factor

Acknowledgements

I would like to thank Curran Crawford for inspiring me to pursue research in the field of energy systems modeling, as well as providing me with the resources and tools necessary to effectively complete this project. I would also like to thank Ned Djilali and David Chassin, along with the many other amazing researchers at the Institute for Integrated Energy Systems at the University of Victoria (IESVic), whom provided valuable insight and a grounded sounding board for my research ideas, as well as their technical implementation. The employees at the Bonneville Power Authority (BPA) and National Renewable Energy Laboratory (NREL) were instrumental in obtaining relevant environmental input data, as were my colleagues at Simon Fraser University and the University of Victoria involved in the CPEVS project. Further, I would like to thank CIMTAN and NSERC for providing funding throughout my studies, without which it would not have been possible.

Finally, I would like to thank my friends and family, for always encouraging my studies while keeping me grounded in reality.

1 Introduction

1.1 Motivation.

As global warming and GHG emissions are becoming a critical issue around the world, there is increasing investment in renewable electrical generation technologies and a shift to electrification of transportation [1]. While there has been a strong push in the development of renewable generation facilities, particularly solar photovoltaic, wind turbine generation, and micro-hydro or run-of-river generation technologies, the infrastructure to support the integration of such inherently variable generation resources is struggling to keep up [2]. Electric utilities must ensure that reliable electricity is constantly available to users when they desire it, and as the penetration of variable renewable generation increases, the stress put on the conventional generation and distribution systems can be pushed to its limits [3]. Further complicating the problem is that electrical demand continues to increase, with BC Hydro projecting a 1.7% annual increase in demand over the next 20 years [4].

One area that exhibits considerable flexibility in addressing the variability of renewable generation, as well as conventional power systems operating requirements, is demand response (DR). Rather than treating electrical loads as strictly must-serve entities, the integration of demand response programs via the smart grid enables the deferral of certain electrical loads to more opportune times. Generally demand response programs are deployed utilizing large commercial and industrial loads as they are of sufficient size to easily integrate into a conventional electrical power system [5], [6]. However, recent work has been completed to show that an aggregate population of residential scale loads, specifically home heating using air source heat pumps, and electric vehicle charging loads, are capable of providing significant ancillary services capacity to electrical system operators [7], [8]. One of the key considerations in this work is that consumer comfort constraints and end-use functionality of the individual appliances must remain a primary objective of the controllers. This ensures that consumers will be willing to participate in the demand response program, and minimizes the inconvenience caused to individual consumers while still maintaining a robust demand response system to the power systems operator.

One of the major hurdles to widespread adoption of residential demand response programs is the cost of communications infrastructure, coupled with individual privacy concerns related to the device-state information being used in the demand response control algorithms [9]. This thesis will examine the ability to implement a demand response program for aggregate populations of residential deferrable loads using limited device-state information from a portion of the participating population. In this manner, it is hoped that widespread adoption and participation in demand response programs will be possible with reduced communications infrastructure costs, and the ability for a subset of a population to participate in the demand response program without reporting any device-state information, thus alleviating privacy concerns.

1.2 Main Contributions

Many control strategies have been implemented in previous works, but some of the most promising appear to be centralized control using aggregators, similar to that described in Parkinson [7]. This thesis will focus on centralized control DR algorithms based on Parkinson's previous work, employing a similar DR control system to provide power systems operators with virtual generation capable of providing ancillary services or renewable energy smoothing. The need for full information of all participating loads is investigated, with an aim to reduce the instrumentation and knowledge requirements for successful DR control. In particular, this thesis offers the following main contributions:

1. The development of a refined computational model capable of simulating various DR algorithms for populations of any number of residential heat pumps and plug-in electric vehicles using either a de-centralized or centralized controller, as well as optimal dispatch among multiple populations for unlimited time periods.
2. A preliminary evaluation of the capacity that load communities of heat pumps and plug-in-vehicles are capable of providing to the grid when employed as regulating reserve virtual generation, and when employed to smooth wind generation injections into the grid.
3. A novel control strategy to accurately manage multiple populations of electrical loads to provide ancillary services to the power system, incorporating limited knowledge of a portion of the population's device-states within the system. This system maintains the ability to simultaneously balance grid-side objectives with the customer comfort-

constraints commonly expected by consumers on the demand-side, while further addressing the privacy concerns of the population.

4. An investigation into the effects of limited device-state information from a sub-group of a load community on its ability to provide effective demand response, and the impacts of the number of responsive loads recruited into such a load community on the available capacity of the demand response program.

1.3 Thesis Structure

This thesis proceeds as follows: **Chapter 2** provides an overview of conventional power systems operation. This chapter identifies a number of challenges associated with the increased penetration of distributed renewable generation resources, and some of the techniques used to address them. In particular, emphasis is placed on demand response programs, including the introduction of a novel demand response approach proposed by Parkinson [7], as it is the theoretical basis for the work presented in this thesis. **Chapter 3** describes the models used to simulate participating loads employed in the subsequent demand response programs. The participating loads modeled are residential heat pumps, and plug-in electric vehicle charging. **Chapter 4** introduces the concept of providing user-constrained demand response capabilities with limited knowledge. A computational framework is developed that permits the provision of ancillary services via demand response from an aggregate load community, even under scenarios where full knowledge of individual load-states is unavailable. The provision of ancillary services, as well as smoothing of wind energy injections into the grid are investigated. **Chapter 5** presents the results of various simulations utilizing these demand response control algorithms, as well as an analysis of the available capacity these load communities can contribute to power systems operation. **Chapter 6** concludes the thesis, providing a summary of key findings and recommendations for future work.

2 Aging Infrastructure and Increasing Demand

The current electrical generation and distribution systems are optimized for large, dispatchable generation facilities that are able to respond to fluctuations in electrical power demand in real-time through frequent throttling of available fast-acting generation resources. This arrangement has worked successfully for many years, however with the increase in non-dispatchable generation it is being pushed to its limits and not operated in the most efficient manner possible [7], [10]. Not only does the operation of generation resources in this manner reduce equipment lifetime, it also results in inefficient operations and increased GHG emissions.

2.1 Conventional Electrical Generation Resources

Canada has a fairly clean energy portfolio, with over 60% of electrical generation being produced from clean sources [11]. However, in order to meet increasing demand additional generation projects will be required in the coming years [4]. The costs associated with a variety of modern generation technologies are summarized in Table 2.1 [7], [12], [13].

Table 2.1 - Cost and Emissions Data for Large-scale Generating Technologies [7], [12], [13].

Technology	Overnight Capital Cost [$/kW]	Fixed O&M Costs [$/kW-yr]	Variable O&M Costs [$/MWh]	Emissions [tCO_2/MWh]
Hydroelectric	$2936	$14.13	0.00	0.009
Nuclear	$5530	$93.28	$2.14	0.012
Coal	$3591	$45.65	$5.85	0.980
CCGT	$825	$7.19	$12.91	0.450
OCGT	$970	$14.27	$3.44	0.650
Wind	$2213	$39.55	$0.00	0.015
Solar PV	$4028	$26.22	$0.00	0.061

As shown in Table 2.1, wind generation has one of the largest initial construction costs of generation technologies, however fuel costs are non-existent and O&M costs are among the lowest. Although both nuclear and hydroelectric generation produce slightly less

lifetime emissions, their initial construction costs are extremely high. Furthermore, there is political, environmental, and societal opposition to both nuclear and large-scale hydroelectric generation projects [14], [15]; and, few feasible locations to implement large-scale hydroelectric projects remain un-utilized throughout Canada [16]. One particular large scale hydroelectric project currently under consideration is the Site C Dam on the Peace River in Northeastern British Columbia. The Site C Dam is one of the last feasible locations for such a project in the Province, and preliminary cost estimates have reached as high as $7000/kW of installed capacity [17]. In addition to higher than average construction costs, there is significant opposition to the Site C Dam project on account of environmental and societal grounds.

These factors, coupled with increased public and political pressure to reduce GHG emissions of new generation projects has resulted in significant increases in development of new renewable energy projects [4], [18]. In particular, BC Hydro has been mandated to increase overall grid system efficiency, with a focus on renewable energy generation projects as a part of the BC Clean Energy Act [4]. However the majority of renewable energy generation technologies being considered are inherently variable in nature, requiring additional investment in infrastructure to ensure reliable integration with the electrical grid.

2.1.1 Renewable Energy: Variable Generation Resources

One of the primary challenges that arises from increased renewable generation into the electrical grid is that it both variable and non-dispatchable. Many renewable generation technologies (solar, wind, tidal, wave, etc.) only produce electricity during periods when their associated resource flux is available – generation output depends on the solar insolation, wind speed, tidal flow, or wave action, respectively. They will generate electricity when the natural resource is abundant, but will reduce or cease to generate any electricity during periods of reduced resource availability. This non-dispatchable generation requires power systems operators to balance load with additional generation by throttling other dispatchable generation resources to compensate. As a result, increased variable renewable energy generation requires significant dispatchable generation capacity to be in place at all times, regardless of whether it is running or simply in standby mode.

One example of the variability of renewable generation, and the resultant temporal mismatch between renewable generation and load profile is shown in Figure 2.1[19].

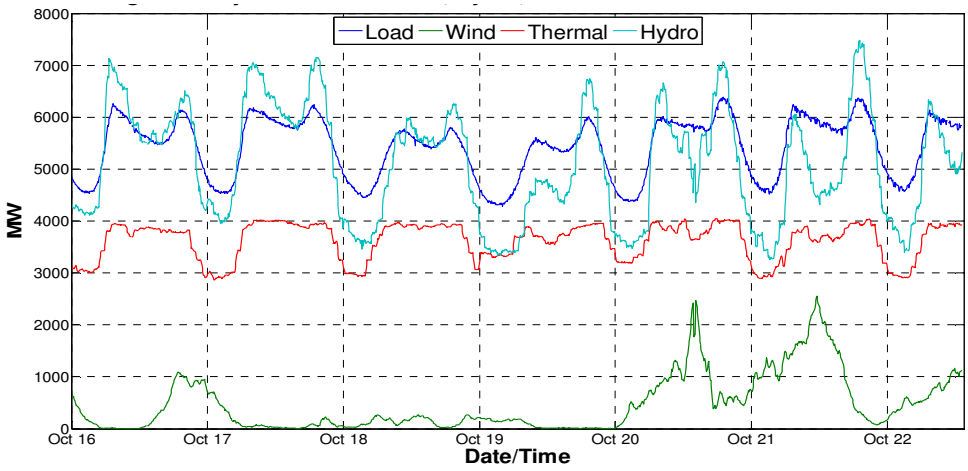

Figure 2.1 – BPA Balancing Authority Load & Total Wind, Hydro, and Thermal Generation 16 Oct 2014 – 23 Oct 2014 [19].

As shown in Figure 2.1, there is no guarantee that the renewable generation will occur at the same time as periods of increased demand. As a result, it is necessary to either store excess energy when it is produced for use at a later time, or to curtail generation when it exceeds demand and rely on dispatchable generation to top-up renewable generation when it does not meet demand. Not only is this operating approach expensive, but it is also inefficient and results in additional GHG emissions from dispatchable generation operating outside of optimal efficiency parameters to match electrical demand and renewable energy generation [7].

2.2 Conventional Power System Operations

The process used by modern utility operators to achieve the required balance between generation and demand is a highly regulated and complex process, spanning operations at the millisecond level up to generation planning studies looking multiple decades into the future. Long-term planning operations are necessary to ensure that adequate generation resources are built to meet anticipated future demand, while daily and hourly bidding operations are used to optimally dispatch available generation resources while reducing operating costs and maintaining system stability.

Electrical generation is generally categorized as one of the following three types to permit modern electrical operations and planning [20]:

1. **Base-load generation** – the slowest responding and largest capacity generation, suitable to provide large quantities of stable power over long time periods. Generally these are large thermal generation facilities, large scale hydroelectric, or nuclear power plants. These facilities run uninterrupted throughout the year with the exception of maintenance shutdowns.
2. **Intermediate generation** - runs essentially continuously, but only during certain periods of the year. It provides additional power to the electrical grid to account for seasonal variations in electrical consumption. And,
3. **Peak generation** - the generation capacity to respond to daily variations in electrical demand. It is fast acting and able to rapidly ramp up and down, but is typically the most expensive generation to operate.

With the integration of variable renewable energy into the electrical grid, the dispatch of peak generation resources becomes more variable to ensure system generation can meet demand. The scheduling and economic dispatch of generation assets within an electrical grid is in itself a complex subject, with many factors affecting the price paid for generation depending on the purpose and capabilities of the generation resource. Typically, however, fast-acting generation resources that can respond to rapid variations in electrical demand are the most expensive generation to purchase at the wholesale level. These resources are commonly referred to as regulating or balancing reserves, and are required due to variations in electrical demand ranging from 1 to 30 minutes – very similar timescales to the commonly observed short-term variability of wind, solar, and wave energy generation [22]. As a result, increased penetration of renewable generation into an electrical grid can result in the need to dispatch greater amounts of regulating or balancing reserves, increasing overall operating costs and GHG emissions [7].

2.3 Addressing Increased Variability of Renewable Generation

There are a number of potential solutions to address the variability that comes with increased renewable generation in the electrical grid, each with its own unique benefits and challenges. Operating dispatchable generation resources to firm-up renewable generation

is effective, but results in additional GHG emissions and increases the costs of renewable generation projects when firming power capacity is taken into consideration [22]. The primary solutions that are robust enough for wide-scale grid integration of variable renewable generation are dedicated energy storage resources, and demand response programs [23], [24]. The following sections will briefly discuss both of these potential solutions as well as some of their benefits and limitations.

2.3.1 Energy Storage Resources

Energy storage resources have seen a surge of development in the last century, resulting in feasible solutions for long-term storage and fast-acting short term storage technologies; however they remain expensive to purchase and operate at utility-scale capacities [25], [26]. Table 2.2 provides a summary of the costs of common storage technologies, as well as their respective round-trip energy efficiencies.

Table 2.2 - Cost of Various Storage Technologies [25].

Technologies	Energy Cost [$/kWh]	Power Cost [$/kW]	Balance of Plant Cost [$/kW or $/kWh]	O & M Cost [$/kW]	Efficiency [%]	Lifetime [years]
CAES	10	450	160 $/kW	6	70	30
PHS	12	2000	2 $/kWh	3	80	40
Pb-acid	300	450	100 $/kW	10	75	6
Li-ion	1500	1500	100 $/kW	10	93	15
Flywheels	1,000	350	100 $/kW	18	90	15
SMES	10,000	300	1,500 $/kWh	10	95	20
EC	30,000	300	100 $/kW	13	95	30

One common theme among grid-scale energy storage technologies is a relatively high combined cost of storage, and a less than ideal efficiency of energy conversion resulting in considerable round-trip energy losses. In addition, these storage facilities must be designed for the largest variations in renewable energy fluctuations, resulting in significant idle storage capacity during normal operation [25]. Despite these limitations, distributed storage has emerged as a viable solution to addressing issues related to variability of renewable generation and grid-side ancillary services [27], [28].

2.3.2 Demand Response Programs

Demand response programs are not new – in fact, they have been implemented historically by power systems operators as a last resort through the practice of systematic load shedding to prevent blackouts [29]. Modern demand response programs have become more elegant, taking into consideration the impacts of the program on end-users, coupled with operating principles to achieve the greatest benefit to the electrical system operator without interfering with the end-use function of the participating. These programs can be broken down into two categories depending on how they interact with participating loads: indirect demand response (price signals), and direct demand response. Each of these types of demand response system can be implemented using a distributed or centralized controller, depending on the system performance desired and operating constraints of the program.

Indirect DR provides control of participating loads without specific knowledge of individual device-states or operating characteristics - one common example being time of use (TOU) pricing schemes, where the cost of electricity is variable throughout the day in response to demand and availability of generation resources. Despite not knowing the specific device-states of participating loads, it is possible for a utility operator to estimate the resultant system response to a specific price signal. This approach can be effective at influencing the demand curve, particularly for peak-shaving or valley-filling objectives [30], [31], however it is often difficult to accurately predict the system response to a change in price signal as it depends on a number of independent and difficult to predict variables [32]. Recent work has been undertaken on this particular issue by Pacific Northwest National Labs, wherein the price signal is incorporated into an autonomous control system using proprietary thermostats and communications infrastructure [20]. This approach interfaces very well with conventional time-of-use utility pricing schemes, while improving the accuracy of the response obtained from an indirect DR program.

Direct demand response provides a much more predictable system response to a control signal by directly influencing device behaviors based on known device-state information. As a result, direct demand response programs require that participating loads are equipped with sufficient communications devices to transmit and receive device-state data and control signals from the demand response system operator. The advantage to direct DR systems is that the response of the participating population is much more accurately known,

and can be controlled to a high degree of precision [33]. The cost of this high degree of predictability and control is that the end-use functionality of the participating devices is more likely to be disrupted if not carefully controlled – customer comfort constraints must be clearly indicated and compensated for in the control algorithm development to ensure the DR program does not produce unacceptable device behavior [34].

Both direct and indirect demand response programs exhibit considerable advantages when compared to energy storage systems for grid-scale applications:

1. The round-trip efficiency of demand response programs can approach 100%, as the deferred energy is stored as the end-use product (home heat, or EV battery charge, for example). This contrasts energy storage systems that have inherent inefficiencies in the energy storage process itself [7], [25].
2. The costs of demand response programs are much smaller than similarly sized energy storage systems, as the loads themselves are utilized as storage mediums. The only additional costs are associated with the communications infrastructure, and is largely already available as smart meters and smart grids are rolled out across North America [34].
3. Demand response programs, particularly aggregate residential load demand response programs are easily scalable, and can be expanded as required by recruiting additional loads to participate in the program [8].

These factors make demand response programs a leading candidate to aid power systems operators in dealing with variable renewable generation, as well as to provide conventional ancillary services to electrical grid operations. It should be noted, however, that while demand response programs are well-suited to provide balancing reserves, they do not provide net energy to the electrical grid, nor are they suitable to directly provide substantial grid stability services at this point in development [20].

In addition to the selection of the type of demand response program, be it direct or indirect, selection of an appropriate control structure is also important in establishing DR resources. Aggregate controllers reduce computational complexity and individual hardware requirements for participating loads, as the computationally intensive portion of the control system is located at a central area. Distributed control, on the other hand, requires individual device controllers to determine the optimal dispatch of each device

independently of other participating loads. This has the advantage of reducing the overall computational complexity of the control system, and distributing tasks among multiple agents in the system, however it comes at the expense of processing time and individual device controller costs.

It may be possible to strike a balance between indirect and direct control through the use of an aggregate control structure in a direct control setting under limited information scenarios. If a sample of a participating population is sampled to determine the anticipated system response, it may be possible to maintain full control authority of the non-reporting loads in the population. This would serve to reduce the instrumentation requirements of a direct demand response approach, while maintaining the benefits of predictable system response.

2.3.3 Demand Response Applications

Demand Response programs have a wide variety of applications in the operation of the electrical power system. The rapid variation of electrical loads is useful from a system balancing perspective, reducing the amount of conventional balancing reserves that must be dispatched to maintain overall energy balance of the grid. In addition to basic energy balance operations, it is also possible to use demand response programs to improve system operations and planning models. A group of responsive loads from a similar geographical area could be used to maintain maximum utilization of transmission lines, as well as to protect distribution equipment from overload conditions. With the correct control algorithms, it is possible to utilize demand response programs for ancillary services, grid stability and security operations, and targeted localized transmission system operation [36]. Even in places like British Columbia, where 90% of generation is from highly dispatchable hydroelectric facilities, demand response programs can be utilized to optimize the transmission and distribution grid assets, as well as provide greater flexibility in optimizing the water levels in reservoirs at hydroelectric facilities than is currently available.

2.3.4 Privacy Concerns in Demand Response Systems

For a load to participate in a direct demand response program, certain details regarding the device-state information must be transmitted to a load aggregator to properly determine the

demand response control signal required to achieve the target objective. Some individuals have privacy concerns associated with providing device-state information to power systems operators or load aggregators, as was particularly evident when BC Hydro began implementing a smart meter program; Some BC Hydro customers were opposed to smart meter infrastructure based on health or privacy concerns and refused to have smart meters installed on their homes [37]. Similar opposition is likely to be encountered in the implementation of direct demand response programs, and is one of the primary motivations for work in this thesis on demand response algorithms under limited feedback scenarios. In addition to privacy concerns, algorithms developed to dispatch a demand response program with limited feedback could also aid in reducing the instrumentation costs for the system, as only a portion of the population would require two-way communication infrastructure.

2.4 Identifying suitable loads for Direct Demand Response

The primary goal for any DR program is increased load flexibility, thus the most important consideration is the types of loads recruited for participation in the program. Loads participating in a DR program must be capable of deferring their operation to opportune times, such as when excess renewable generation is available or during periods of reduced total system demand [7]. In addition, the deferral of load operation must result in minimal impacts on customer comfort constraints to ensure that participants are willing to engage in the demand response program. Identifying loads that meet these criteria, and have sufficient capacity to provide useful demand response capabilities, is the first step in implementing demand response programs.

As most demand response programs are aimed at providing ancillary services to power systems operators, or minimizing the variability of renewable generation resources, they must be of a sufficient capacity to participate in these markets [38]. The California Independent System Operator (CAISO), for example, requires participants in the regulating reserve market to provide a minimum of 1 MW of capacity. As most residential loads are an order of magnitude lower than this threshold, it is necessary to recruit and control multiple aggregated loads to achieve these minimum capacity requirements. In addition to

this threshold value, a sufficiently large population is necessary to ensure sufficient load diversity to permit effective control of the aggregate population [39].

Two primary types of load have been identified as having significant potential for participation in residential scale aggregate demand response programs: Thermostatically controlled loads, and energy-constrained storage [7], [29]. The following sections will investigate the specific operational constraints of these loads, as well as the relative usefulness they offer for demand response programs.

2.4.1 Thermostatically controlled loads

Thermostatically controlled loads comprise a large portion of the residential and commercial demand profile [38]. Common examples of residential thermostatically controlled loads include refrigerators, heat pumps, air conditioners, and hot water heaters. These loads operate by switching a machine capable of converting electrical energy to heat energy, and are generally controlled with a thermostat to maintain a user-specified temperature of a conditioned space. Once the initial setting of the thermostat is defined, user-interactions with the devices are relatively rare, and the devices operate autonomously [7].

Thermostatically controlled loads are generally operated in a binary manner, switching between the active- and inactive-states repeatedly in response to thermostat control signals. The operational state of the TCL is described by n, and when active, the device operates at its full power rating P_r. This operational pattern results in a load demand trajectory described by equation (2.1):

$$\boldsymbol{P(t) = n(t)P_r} \tag{2.1}$$

Cycling of TCLs between the active and inactive states occurs when the heat transfer rate from the conditioned thermal system $\dot{q}_{loss}$ is less than the rated heating power of the device [7]:

$$\boldsymbol{\eta|P_r| > |\dot{q}_{loss}|} \tag{2.2}$$

Where η is the coefficient of performance, or efficiency, of the device. This deferrable operation of TCLs makes them ideal candidates for demand response programs, as the thermal energy stored in the conditioned space is generally sufficient to permit 'coasting'

through prescribed intervals with minimal deviations to the resultant space temperature profile [7].

While most TCLs are suitable for demand response programs, residential HVAC systems show the greatest promise of typical residential loads: They are typically among the largest loads in a home, and as such the communications and instrumentation costs would be lower on a per-unit energy basis than other smaller TCLs. Further, electrically powered HVAC devices, such as heat pumps and baseboard electric heaters, are extremely common in temperate climates such as the Pacific Northwest of North America [39]. One drawback to the use of home HVAC devices in demand response programs is that their operation is directly dependent on outdoor air temperature conditions. In the case of TCLs primarily utilized for heating a conditioned space, their flexibility will be reduced during warmer seasons or during periods when the outdoor air temperature approaches the thermostat temperature setting. This could be partially countered through the recruitment of a population of TCLs used for both heating and cooling, such as heat pumps, however there will still remain certain environmental conditions during which the loads show reduced opportunities for deferral. Despite this limitation, TCLs remain one of the most appealing loads for recruitment into a demand response program.

2.4.2 Energy storage as a deferrable load

Another load class that exhibits significant promise for use in demand response programs is energy storage, such as the charging of device batteries or the production of an alternative fuel [7]. The primary function of such loads is to provide a desired level of stored energy at the end of a charging cycle. Further, these loads are rapidly becoming more common, ranging from consumer electronic devices to plug-in electric vehicles. The charging trajectory, E, of such devices can be described by equation (2.3):

$$\boldsymbol{E(T_s) = \int_0^{T_s} \eta P_r n(t) dt \geq E_c; \quad E(0) = 0} \tag{2.3}$$

where η is the one-way conversion efficiency associated with the storage unit, P_r is the rated power of the charger, n is the device operational state at time t, and T_s is the charging cycle duration [7]. From this equation it can be shown that it is possible to fully charge the device in less time than the user specifies if the charger capacity is sufficiently large:

$$\eta P_r > \frac{E_c}{T_s} \quad (2.4)$$

Like TCLs, this characteristic permits deviations from the standard operational-state trajectory, providing the ability to modify the demanded load of the device over the user-set charging-horizon, without affecting device functionality.

Once again, owing to their relatively large capacity, plug-in electric vehicle charging is the most promising residential scale energy-constrained storage load for demand response programs [7], [40]. Significant research has been conducted on the potential of PEVs to provide ancillary services, particularly with respect to vehicle-to-grid energy services [41], [42]. However with current battery technologies, the losses associated with round-trip conversion efficiencies, and the accelerated degradation of battery performance from increased cycling, makes vehicle-to-grid programs less appealing to consumers [7].

Previous research on the use of PEVs in the provision of ancillary services has found that vehicle-to-grid operation is not required to achieve appreciable results; simple deferral of charging processes can provide significant benefits on its own, with increased efficiency owing to only one-way conversion and no detrimental effects on battery performance [7]. Furthermore, BC Hydro projects the market share of PEVs to increase steadily, approaching 5% in 2020 and 20% by 2028 [4]. Another significant advantage to utilizing PEV charging as a demand response resource is that there are only minor variations in driving usage patterns throughout the year [43], resulting in a load population that should maintain diversity and availability regardless of the season.

2.4.3 Hysteresis control of deferrable loads

Device level control of both TCLs and PEV charging is required to ensure that user comfort preferences are maintained, and machinery operational constraints and duty cycles are not exceeded when incorporated into a demand response program.

In the case of TCLs, device level control is typically achieved through the use of a thermostat. As temperature measurements are often accompanied by a considerable amount of volatility, thermostats frequently employ a hysteresis control logic [7]. Hysteresis control involves the definition of a deadband space, or a region of end-use measurements, where no change to the operational state of the device will occur. Measurements outside of

the deadband space will result in a transition from either the active or inactive device state, depending on the current device state. This approach minimizes the frequency of cycling of the device, preventing premature degradation of the machine while maintaining user-defined comfort constraints.

This hysteresis control can be represented mathematically for heating operation as [44]:

$$\boldsymbol{n[k+1]} = \begin{cases} \mathbf{1} & \boldsymbol{\epsilon[k] \leq \epsilon_{-}} \\ \mathbf{0} & \boldsymbol{\epsilon[k] \geq \epsilon_{+}} \\ \boldsymbol{n[k]} & \boldsymbol{otherwise} \end{cases} \quad \textbf{(2.5)}$$

Where ϵ is the normalized end-use state measurement, ϵ_{-} is the lower deadband boundary, $\epsilon_{+}$is the upper deadband boundary, and k is the thermostat sampling index [7]. If the deadband width is defined as δ, the deadband boundaries are defined as:

$$\boldsymbol{\epsilon_{\pm}} = \pm\frac{\boldsymbol{\delta}}{\mathbf{2}} \quad \textbf{(2.6)}$$

The normalized end-state for heat pumps is defined as:

$$\boldsymbol{\epsilon[k]} = \frac{\boldsymbol{\theta_a[k] - \theta_s[k]}}{\boldsymbol{\delta}} \quad \textbf{(2.7)}$$

where θ_a is the indoor air temperature measurement, and θ_s is the user-defined temperature set-point. When a measured end-state value is outside the deadband region, the controller will switch the operational state of the TCL. Specifically, for end-state measurements less than ϵ_{-} the controller will cause TCLs in the inactive-state to transition to the active-state; end-state measurements greater than ϵ_{+} will cause the TCLs in the active-state to transition to the inactive-state [7].

Callaway and Hiskens have suggested that device-level hysteresis controllers can also be used to control Energy-constrained storage [45]. Analogous to sampling the temperature of the conditioned space in TCLs, controllers for energy-constrained storage must sample the current charge level with respect to the minimum charging trajectory that will ensure the device is fully charged at the end of the user-defined charging period. This charging trajectory E_s can be defined according to equation (2.8) [7]:

$$\boldsymbol{E_s[k+1] = E_s[k] + \frac{E_c}{T_s}T;} \qquad \boldsymbol{E_s[0] = 0} \quad \textbf{(2.8)}$$

Comparison between the charging trajectory E_s and the actual device state-of-charge E permits the application of a hysteresis controller to govern the operational-state of the charger. The normalized end-state measurement for energy-constrained storage charging can be determined by equation (2.9):

$$\epsilon[k] = \frac{E[k] - E_s[k]}{E_c} \tag{2.9}$$

2.5 Managing Aggregate Load Demand

It is important to consider a framework for the organization and management of aggregate load communities engaged in demand response programs. As an aggregate load community is necessary to address the technical requirements of ancillary services when recruiting residential scale loads, an intermediary agent to oversee operation of the aggregate load community in the context of the overall power systems operations is necessary. As described by Parkinson, the intermediary should display four attributes to be successful: It must be **non-invasive**, **secure**, **profitable**, and **ecological** [7]. Load management programs that exhibit these four attributes will be more appealing to both recruited loads and power system operators.

While it would be relatively straightforward to permit power systems operators to take responsibility for operating these intermediaries, Parkinson argues that separating the intermediary at the community-level is a superior approach [7]. This approach greatly simplifies network privacy, as individual device-state information need not be transmitted to the power systems operator directly and is only send to the level of the load aggregator. In addition, it would provide a distinct separation between the service provider (the load aggregator), and the power systems operator that is directly benefiting from the services of the demand response program. Further, previous work has shown that the error associated with multiple smaller communities is essentially equivalent to the error observed in a single larger community [8] – however the multiple smaller community approach has the added benefit of reduced network congestion and decreased computational time at each time-step [7]. As a result, a balance must be struck to ensure load communities are sized to ensure computational time is maintained below the time-step employed in the demand response

program while producing a large enough aggregate capacity to be useful in power systems operations.

A group of recruited loads participating in a demand response program, herein referred to as the load community (LC), would be organized by an intermediary agent to provide ancillary services to the power systems operator. This intermediary is referred to as a load aggregator (LA), and would coordinate interactions between the LC to achieve the contracted response desired by the power systems operator [7]. The LA provides a specified deviation from the steady-state load trajectory of the LC at the request of the power systems operator in a format similar to conventional generation. This operation is referred to as a virtual generator model (VGM) throughout this thesis, and preserves the separation between the individual loads in the LC from the power systems operator.

2.5.1 Controlling Load Community Dynamics

While the previously described component-level controls ensure normal device operation is maintained for both TCLs and EV charging, it is necessary to implement a system-level strategy to manage these large populations of participating loads effectively. The approach utilized by Parkinson for system-level control is implemented in this thesis, as described in the following section [7].

In this formulation, device-level hysteresis controllers maintain normal operating limits of TCLs and energy-constrained storage devices. This system-level approach eliminates the need to track individual device operating constraints, significantly reducing complexity and communications requirements. Aggregate population dynamics are then described by the power density distribution functions for the active and inactive machine-states, ϕ_1 and ϕ_0, respectively. The aggregate load is thus defined by the total power existing in the active state, and can be related to the total power in the current responsive population P_{cap} and a capacity factor Φ as [7]:

$$\boldsymbol{P(t) = \sum_{i=1}^{N_i(t)} P_{r,i} \int_{-\infty}^{\infty} \phi_1(\epsilon, t) d\epsilon = P_{cap}(t)\Phi(t)} \qquad \textbf{(2.10)}$$

It is shown by Parkinson that, due to a discontinuity introduced by the device-level hysteresis control logic given in (2.5), that it is possible to control the capacity factor

according to equation (2.11) through a perturbation u to the end-use state comparison [7], [45].

$$\lim_{t_+^* \to t^*} \Phi(u, t_+^*) = \lim_{t_-^* \to t^*} \left\{ \int_{-\infty}^{\epsilon_- + u(t_-^*)} \phi_0(\epsilon, t_-^*) d\epsilon + \int_{-\infty}^{\epsilon_+ + u(t_-^*)} \phi_1(\epsilon, t_-^*) d\epsilon \right\} \quad \textbf{(2.11)}$$

This control is achieved by modifying the state-transition boundary locations, and requires that each element within the targeted population is equipped with suitable communications hardware, such as programmable communicating hysteresis controllers (PCH) [45]. This effectively modifies the device-level hysteresis control logic introduced in (EQ) to the form given by:

$$n_i[k+1] = \begin{cases} 1 & \epsilon[k] \le \epsilon_- + u[k] \\ 0 & \epsilon[k] \ge \epsilon_+ + u[k] \\ n_i[k] & otherwise \end{cases} \quad \textbf{(2.12)}$$

By synchronizing loads near state-transition boundaries, the controller is able to influence aggregate population dynamics. This approach ensures that in the case of deferrable energy storage, energy is never extracted from the unit to achieve the desired response [7].

To enable this control, each participating load equipped with a PCH provides the LA with its current power-state vector z_i. The loads then wait for the system-level set-point decision prior to evaluating the revised hysteresis control logic of (2.12). This sequence of events ensures that individual device sampling intervals are synchronized to the same central clock, permitting the system-level controller to schedule these loads in real-time. The power state vector, z_i, reported by individual loads to the system-level controller includes the device state, the normalized end-state measurement value, and the power rating of the device:

$$z_i[k] = \begin{bmatrix} n_i[k] \\ \epsilon_i[k] \\ P_{r,i} \end{bmatrix} \quad \textbf{(2.13)}$$

Which, when multiple loads are participating in the demand response program, results in the LA receiving a set of power-state vectors Z from the participating loads:

$$Z[k] = \{z_1[k], z_2[k], \dots, z_{N_i}[k]\} \quad \textbf{(2.14)}$$

This control approach results in the closed-loop control strategy depicted in Figure 2.2[7].

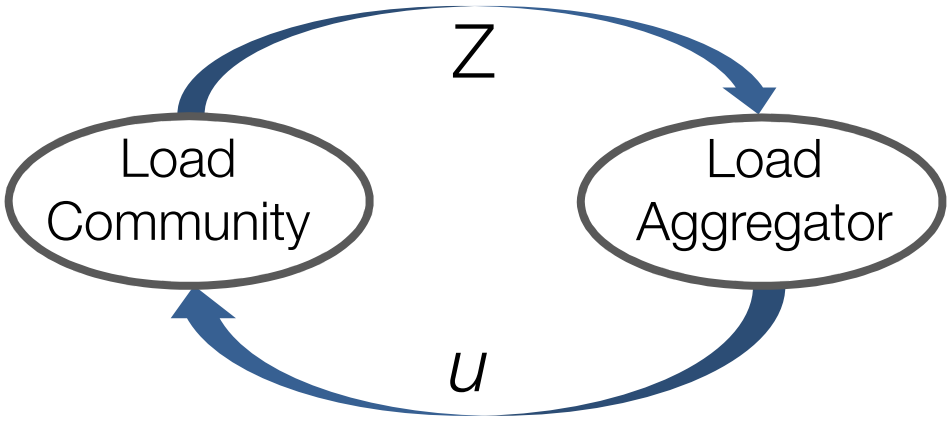

Figure 2.2 - Closed-loop control strategy implemented.

For this control strategy to be successful, the delay-time between the LA signal broadcast and LC response must be considerably less than the PCH update time. This delay-time is directly related to the number of participating loads, network quality, and efficiency of system-level decision-making [7]. This is another factor influencing the preference for multiple moderately sized LCs as opposed to a single LC with a very large number of participating loads.

Provided that the device-level controllers operate at the same measurement resolution, $\mathcal{R}$, it is possible to determine the populations demand response as a function of the end-use state comparison perturbation u_s:

$$\boldsymbol{P_{cap}}[\mathbf{k}+\mathbf{1}]\boldsymbol{\Phi}[\boldsymbol{u_s}, \boldsymbol{k}+\mathbf{1}] = \sum_{i=1}^{N_i} \boldsymbol{P_{r,i}} \left[\sum_{-\infty}^{u_s+\epsilon_-} \boldsymbol{\phi_0}[\boldsymbol{\epsilon}, \boldsymbol{k}] + \sum_{-\infty}^{u_s+\epsilon_+} \boldsymbol{\phi_1}[\boldsymbol{\epsilon}, \boldsymbol{k}] \right] \qquad \textbf{(2.15)}$$

Where u_s may only take on values according to the device-level controller measurement resolution within a specified range ($|u[k]| \leq \delta/4$) to prevent rapid cycling of devices, and discretized according to the device-level controller resolution as in (2.15):

$$\boldsymbol{u[k]} = -\frac{\boldsymbol{\delta}}{\mathbf{4}} + \boldsymbol{m}\frac{\boldsymbol{\delta}}{\mathbf{2}\boldsymbol{\mathcal{R}}} \quad ; \quad \boldsymbol{\mathcal{R}} \in \mathbb{N} \qquad \textbf{(2.16)}$$
$$\boldsymbol{m} = \mathbf{0}, \mathbf{1}, \mathbf{2}, \dots, \boldsymbol{\mathcal{R}}$$

The resultant function (2.17) is convex, and as such it can be implemented by the LA into a deviation minimization problem [7]:

$$\boldsymbol{Min}(\boldsymbol{P^*}[\boldsymbol{k}+\mathbf{1}] - \boldsymbol{P_{cap}}[\mathbf{k}+\mathbf{1}]\boldsymbol{\Phi}[\boldsymbol{u_s^*}, \boldsymbol{k}+\mathbf{1}])^2 \qquad \textbf{(2.17)}$$

Where the optimal perturbation u_s^* will result in an aggregate responsive load demand equivalent to the specified target P^*. To ensure the desired response of the aggregate responsive load population is achieved, the specified target must exist within the feasible region defined by:

$$\begin{gathered} P_{min}[k+1] \leq P^*[k+1] \leq P_{max}[k+1] \\ P_{max}[k+1] = P_{cap}[k+1]\Phi[u_{max}, k+1] \\ P_{min}[k+1] = P_{cap}[k+1]\Phi[u_{min}, k+1] \end{gathered} \quad \textbf{(2.18)}$$

This feasible region defines the limitations of the VGM, corresponding to the virtual generator ramp-rate at each time-step. As the load populations are dynamically evolving in time, it is necessary to implement a closed-loop control strategy to ensure the LA can accurately report the LCs capabilities as a VGM for each time-step.

2.5.2 Dispatch of multiple loads

The tracking error associated with multiple smaller LCs is found to be roughly equivalent to the error associated with a single large LC containing the same total number of individual loads [8]. This phenomenon, in conjunction with the need to maintain low computational time of the system-level controller, provides incentive for a LA to distribute recruited loads into multiple smaller VGMs rather than a single large model for each load type. Furthermore, if a LA intends to manage different types of loads, it can reduce complexity and improve system performance by developing individual VGMs for each type of load.

However, when operating multiple VGMs the LA must determine the optimal dispatch of each VGM to achieve the global LA target response. It is preferable for the LA to minimize the variability and magnitude of the end-use state comparison perturbation u [7]. Minimizing the magnitude of the perturbation serves to reduce the deflection from the customers' set-point values, and minimizing the variability of the perturbation accelerates the dispersion of end-use states within the system-level equivalent deadband space. Greater dispersion of end-use states results in a larger feasible space for the VGM, providing additional flexibility in achieving the desired response of the power system operator.

By assuming that the amplitude of the control signal will be proportional to the amplitude of the deflection of the LC from the uncontrolled trajectory, computational time can be reduced by implementing a linear programming approach [7]. The uncontrolled trajectory

is equivalent to a trajectory with a perturbation of $u_s[k] = 0$, and also represents the lowest variability and amplitude control signal possible:

$$\boldsymbol{P_0[k+1] = P_{cap}[k+1]\Phi[(u_s = 0), k+1]} \quad \textbf{(2.19)}$$

Denoting the controlled deviation from P_0 as ΔP^*, and dropping the time-dependence, the responsive load trajectory is given by:

$$\boldsymbol{P^* = P_0 + \Delta P^*} \quad \textbf{(2.20)}$$

The boundary conditions that govern the controlled deviation from the uncontrolled trajectory are based on the maximum allowable set-point changes defined previously to prevent rapid cycling of machines:

$$\begin{aligned} \Delta P^*(u = 0) &= 0 \\ \Delta P^*(u = \delta/4) &= P_{max} - P_0 \\ \Delta P^*(u = -\delta/4) &= P_0 - P_{min} \end{aligned} \quad \textbf{(2.21)}$$

Although the relationship between these boundary conditions may not be linear, a reasonable first-order approximation is to assume the deflections in either direction are proportional to the ratio of the controlled deflections and their maximums [7]:

$$\begin{aligned} u &= \frac{\delta}{4}\frac{\Delta P^*}{P_{max} - P_0} \quad P_T > \sum_{p=1}^{N_p} P_0^{(p)} \\ u &= \frac{\delta}{4}\frac{\Delta P^*}{P_0 - P_{min}} \quad P_T < \sum_{p=1}^{N_p} P_0^{(p)} \end{aligned} \quad \textbf{(2.22)}$$

Where P_T is grid-side objective target for a LA dispatching N_p responsive load communities within the control area. The LA may then attempt to minimize control signal deflections, while attempting to meet the grid-side objective target without violating any individual VGM ramp constraints. Depending on the magnitude of the grid-side objective target, and the aggregate uncontrolled trajectory of all participating loads, one of two linear programming formulations are utilized:

$$\begin{aligned} &\textbf{Min} \sum_{p=1}^{N_p} \frac{\Delta P^*}{P_{max}^{(p)} - P_0^{(p)}} \\ \textbf{s.t.} \quad &\sum_{p=1}^{N_p} \Delta P^{*(p)} = P_T - \sum_{p=1}^{N_p} P_0^{(p)} \\ &\Delta P^{*(p)} \leq P_{max}^{(p)} - P_0^{(p)} \\ &\Delta P^{*(p)} \geq 0 \end{aligned} \tag{2.23}$$

$$\frac{\Delta P^{*(p)}}{P_T} = \frac{P_{max}^{(p)} - P_0^{(p)}}{\sum_{p=1}^{N_p} (P_{max}^{(p)} - P_0^{(p)})}$$

When P_T is greater than the aggregate uncontrolled trajectory, and:

$$\begin{aligned} &\textbf{Min} \sum_{p=1}^{N_p} \frac{\Delta P^*}{P_0^{(p)} - P_{min}^{(p)}} \\ \textbf{s.t.} \quad &\sum_{p=1}^{N_p} \Delta P^{*(p)} = P_T - \sum_{p=1}^{N_p} P_0^{(p)} \\ &\Delta P^{*(p)} \leq P_0^{(p)} - P_{min}^{(p)} \\ &\Delta P^{*(p)} \geq 0 \end{aligned} \tag{2.24}$$

$$\frac{\Delta P^{*(p)}}{P_T} = \frac{P_0^{(p)} - P_{min}^{(p)}}{\sum_{p=1}^{N_p} (P_0^{(p)} - P_{min}^{(p)})}$$

When P_T is less than the aggregate uncontrolled trajectory.

Solving the linear programming formulation for the controlled deviations of each population will ensure that the desired grid-side objective target can be attained, while simultaneously minimizing the amplitude of the control signal u across each load-type. It is imperative that the grid-side objective target is feasible for the participating LCs to ensure a valid solution to the linear programming formulation is possible.

3 Computational Modeling Framework

This chapter describes the specific computational models that are employed to simulate the various loads that comprise the load communities participating in the demand response program.

3.1 Demand-side: Load Models

Demand-side load models must be capable of accurately simulating individual device dynamics with minimal computational power. The following sections explain the dynamic load models used to simulate the targeted end-use devices: Residential air-source heat pumps, and plug-in electric vehicle charging.

3.1.1 Heat Pump Equivalent Thermodynamic Parameter Model

The study of building heating systems, such as air-source heat pumps, and their interactions with building characteristics commonly results in the application of detailed multi-physics approaches [7]. Due to the computational complexity of such simulations, they are not suitable for modeling large populations of individual buildings as required for demand response programs utilizing residential scale loads. A simplified model structure commonly employed in such demand response simulations is the equivalent thermal parameter (ETP) model [7], [8], [46].

The ETP model represents each building as a combination of thermal masses, which are linked to one another via their related coefficients of heat transfer. Previous works have employed a simple ETP model incorporating two coupled thermal masses to represent small- to medium-sized buildings such as residential homes in North America [47]. This coupled thermal system divides the home into two thermal masses: the thermal mass of the air inside the dwelling C_a, and the thermal mass of the building structure C_m. These thermal masses are then permitted to interact with the outdoor air temperature θ_a through the building envelop thermal resistance R_{ao}. The resulting temperature trajectories of the two thermal masses are then coupled through the following linear dynamic system representation:

$$\begin{bmatrix} \dot{\theta}_a \\ \dot{\theta}_m \end{bmatrix} = \mathbf{A}\begin{bmatrix} \theta_a \\ \theta_m \end{bmatrix} + \mathbf{B}\begin{bmatrix} \theta_o \\ \dot{q} \end{bmatrix} \quad \textbf{(3.1)}$$

Where θ_m is the building contents temperature, and the system inputs are represented by the outdoor air temperature θ_o, and the heat input $\dot{q}$. The heat input used in this model is based on the heating power of the heat pump $\dot{\boldsymbol{q}}_{\boldsymbol{op}}$, and the operational state of the heat pump is determined by the hysteresis controller presented in section 2.4.3.

$$\dot{\boldsymbol{q}} = \boldsymbol{n}(\boldsymbol{t})\dot{\boldsymbol{q}}_{\boldsymbol{op}}(\boldsymbol{t}) \quad \textbf{(3.2)}$$

The state- and input- transformation matrix, **A** and **B**, are determined from the structure of the ETP, which is presented below in Figure 3.1 [7].

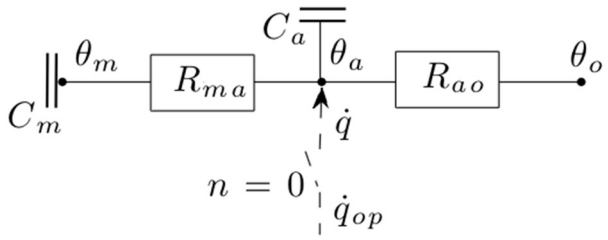

Figure 3.1 - ETP Schematic [7].

$$a_{11} = -\left(\frac{1}{R_{ma}C_a} + \frac{1}{R_{ao}C_a}\right) \quad a_{12} = \frac{1}{R_{ma}C_a} \quad a_{21} = \frac{1}{R_{ma}C_m} \quad a_{22} = -\frac{1}{R_{ma}C_m}$$

$$b_{11} = \frac{1}{R_{ao}C_a} \quad b_{12} = \frac{1}{C_a} \quad b_{21} = 0 \quad b_{22} = 0$$

$$\mathbf{A} = \begin{bmatrix} a_{11} & a_{12} \\ a_{21} & a_{22} \end{bmatrix} \quad \mathbf{B} = \begin{bmatrix} b_{11} & b_{12} \\ b_{21} & b_{22} \end{bmatrix} \quad \boldsymbol{\theta} = \begin{bmatrix} \theta_a \\ \theta_m \end{bmatrix} \quad \mathbf{U} = \begin{bmatrix} \theta_o \\ \dot{q} \end{bmatrix}$$

$$\dot{\boldsymbol{\theta}} = \boldsymbol{A\theta} + \boldsymbol{BU} \quad \textbf{(3.3)}$$

A solution to the resultant discrete-time version of (3.3) under steady inputs is [48]:

$$\boldsymbol{\theta}[\boldsymbol{k}+\mathbf{1}] = \boldsymbol{\Omega\theta}[\boldsymbol{k}] + \boldsymbol{\Gamma U}[\boldsymbol{k}]$$
$$\Omega = \exp(\boldsymbol{AT})$$
$$\Gamma = \int_0^T \boldsymbol{\Omega B} d\tau \quad \textbf{(3.4)}$$

Where Ω is the state-transition matrix, and Γ is the input-transition matrix. Because the diurnal variations of outdoor temperature that affect device-level duty-cycles are much longer than typical thermostat sampling frequencies, the utilization of temperature data

with a 1-minute resolution is reasonable [7]. Additional system internal gains and losses (such as opening and closing doors, solar gains, air infiltration, and the operation of other loads) are modeled with a white noise term, **e**, which is assumed to be normally distributed with variance σ, and included in the component model utilized in this thesis according to equation (3.5):

$$\boldsymbol{\theta}[\boldsymbol{k}+\mathbf{1}] = \boldsymbol{\Omega\theta}[\boldsymbol{k}] + \boldsymbol{\Gamma U}[\boldsymbol{k}] + \boldsymbol{e}[\boldsymbol{k}] \tag{3.5}$$

3.1.1.1 Heat Pump Unit Sizing

To accurately model a representative population of homes, the heat pump unit sizing must be suitable for the houses being simulated. To ensure reliability, the approach presented by Parkinson was used for heat pump unit sizing [7]. This technique incorporates worst-case scenario estimates of the parameters of the ETP model, in combination with the most extreme environmental temperatures anticipated for the desired study area, to size heat pumps for each modeled home. This is accomplished by balancing the heat flux from the house that occurs under these conditions to maintain the indoor air temperature set-point with the design heating power of the heat pump, and an appropriate oversizing factor. As such, the design heating power of the heat pump can be determined using equation (3.6), where γ is the over-sizing factor, θ_s is the thermostat set-point temperature, and θ_d is the heating design temperature.

$$\dot{\boldsymbol{q}}_{\boldsymbol{d}} = \boldsymbol{\gamma}\left(\frac{\boldsymbol{\theta_s} - \boldsymbol{\theta_d}}{\boldsymbol{R_{ao}}}\right) \tag{3.6}$$

The variable efficiency of air-source heat pumps was addressed by fitting a third order polynomial to the air-temperature efficiency curves from a manufacturer's datasheet [49]. As a result, the power rating of individual units can be determined using the efficiency of the heat pump at the design temperature, η_d:

$$\boldsymbol{P_h} = \frac{\dot{\boldsymbol{q}}_{\boldsymbol{d}}}{\boldsymbol{\eta_d}} \tag{3.7}$$

From equation (3.7), the required electrical power to produce the design heating power is P_h. This value was then rounded up to the nearest 0.5 kW to account for discretization between units and conventional air-source heat pump availability [7], [49]. Under all but the most extreme cold temperatures for the region, the heat pump will thus have excess

available capacity, and will cycle between the on and off states to maintain the indoor air temperature according to equation (3.8).

$$\dot{q}_h = \eta[k]P_h \tag{3.8}$$

A fan is used to circulate the heat produced by the heat pump throughout the building, which also contributes to the operational capacity of the device. As a result, the operational heat flux from the heat pump is the sum of the heat from the heat pump, and the additional energy imparted by the operation of the fan.

$$\dot{q}_{op}[k] = \dot{q}_h[k] + \dot{q}_{fan} \tag{3.9}$$

Assuming that the fan operates at an ideal efficiency, the total electric power associated with the operational heat pump is then calculated by:

$$P_r = P_h + P_{fan} \tag{3.10}$$

3.1.1.2 Heat Pump ETP Model Example

A simple example considering a single building is presented to demonstrate the device-level dynamics of the ETP model. The parameters implemented in the model can be found in [50] and [51], and are summarized below in Table 3.1 [7].

Table 3.1 - Parameters implemented in the heat pump ETP model.

Parameter	Description	Value
C	Average thermal capacitance	10 kWh/°C
C_m	Indoor contents thermal mass	75% of C
C_a	Indoor air thermal mass	25% of C
R_{ma}	Indoor heat transfer resistance	0.5°C/kW
R_{ao}	Envelope thermal resistance	2°C/kW
$\dot{q_{fan}}$	Heating power of fan	500 W
θ_s	Temperature set point	20°C
δ	Temperature deadband width	1°C
T	Sampling time interval	1 minute
e	Noise standard deviation	0.01°C $s^{-1/2}$

The outdoor air temperature profile is shown in the top panel of Figure 3.2; the building air- and contents-temperatures in the middle panel, and the device power requirements in the bottom panel.

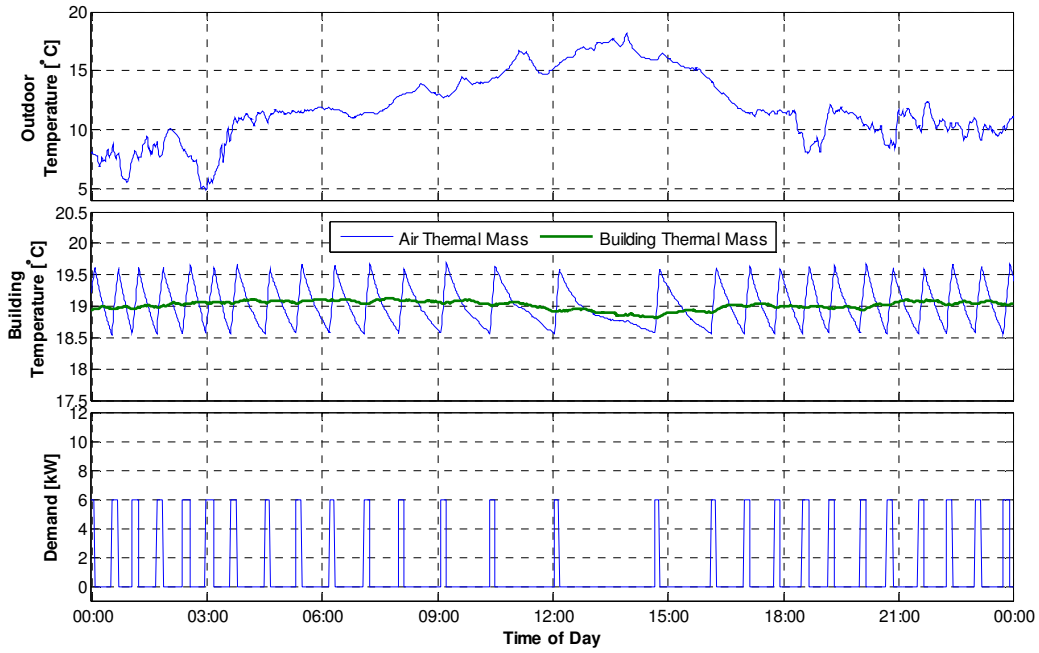

Figure 3.2 - Example of the ETP model response under the displayed outdoor temperature profile.

It is clear from this figure that the device cycles between on- and off-states in response to the indoor air temperature traversing the deadband region. The transition of the building air temperature through the deadband region is influenced by the outdoor air temperature, traversing the deadband region more quickly during periods of colder temperatures.

3.1.2 Plug-in Electric Vehicle charging Model

The electrical demand associated with plug-in electric vehicle (PEV) charging is directly related to the travel history of the vehicle, which can vary widely among potential users due to a multitude of social factors. This large variance in travel history produces significant variability in electric vehicle charging electrical demand, however once the charging time and energy requirements are defined, a simple linear charging model can identify real-time electrical demand for PEV charging. The three key parameters required

for such a model are the desired battery charge capacity, the time that charging begins, and the duration of time available before the desired battery charge capacity is required (charging time).

By neglecting the travel history of the vehicle, and representing it simply as the required battery charge capacity (which can be extrapolated to travel history), it is possible to model the plug-in electric vehicle charging using a simplified linear model [7].

To determine the aggregate electrical load for a community of PEVs, a quasi-steady state model of the charging reaction was implemented to simulate the device-level charging controller. To account for the intrinsic heat loss to the environment during charging, a defined charging efficiency, $\boldsymbol{\eta}$, is employed. The resultant state-equation for the charging-trajectory is thus:

$$\boldsymbol{E[k+1] = E[k] + n[k]\eta P_r T + e[k]} \qquad \textbf{(3.11)}$$

Where the error term, e, is included to represent all un-modeled physical phenomena (ambient temperature changes, transient electrochemical effects, etc.) and takes on a magnitude of constant variance σ [7].

3.1.2.1 PEV Charging Model Example

A simple example considering the charging of a single plug-in electric vehicle is presented to demonstrate the device-level dynamics of the EV charging model. The parameters implemented in the model are based on average values from CPEVS survey data [52] and previous work by Parkinson [7], as summarized in Table 3.2.

Table 3.2 - Parameters implemented in the EV charging model.

Parameter	Description	Value
P_r	Rated power of the charger	5 kW
η	Charging efficiency	0.95
E_c	Desired charging capacity	11 kWh
T_s	Desired charging duration	6 hours
δ	Hysteresis control deadband	0.0025
T	Sampling time interval	1 minute
e	Noise standard deviation	0.01 kW

The hysteresis controller defined in section 2.4.3 provides device level control, resulting in a duty-cycle-based charging rate and the resultant staggered charging trajectory [7]. The selection of the device deadband width governs the duration of the active charging periods, and with δ=0.025 in this example the operational periods last between about 20 and 30 minutes. The charging trajectory using the above parameters is shown in the top panel of Figure 3.3. The middle panel shows the end-use state values of the hysteresis controller, and the bottom panel shows the electrical demand from the charger.

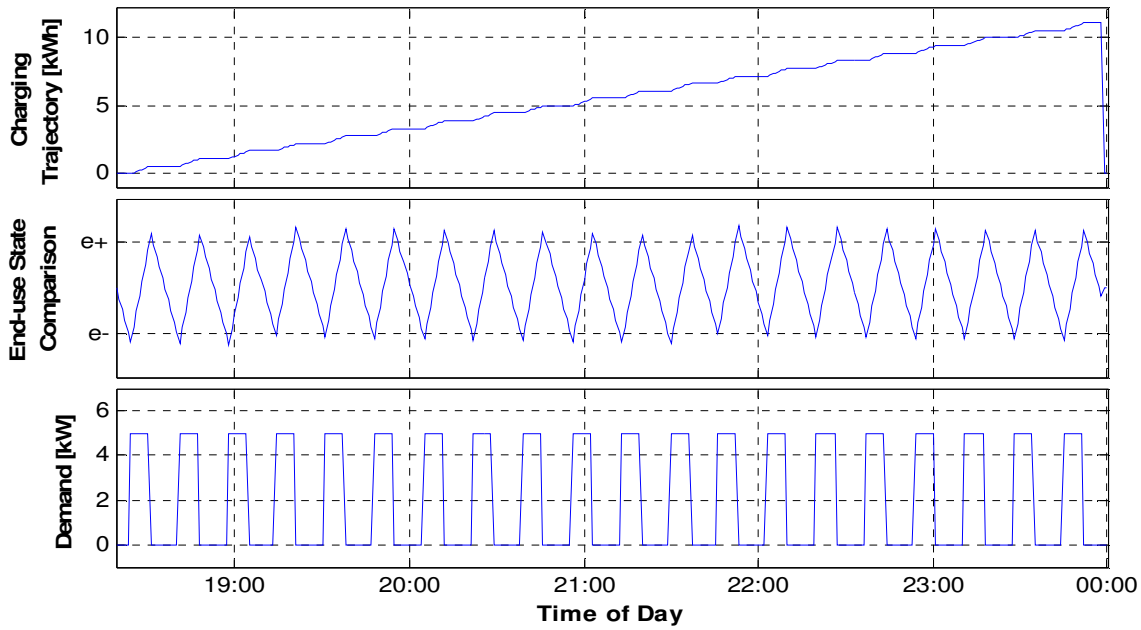

Figure 3.3- Example of the EV load model.

The PEV charging model also includes parameters to simulate vehicles joining and leaving the load community, as well as access to daytime charging. Daytime charging is simulated by creating a second 'virtual' PEV participant, with charging capacity equivalent to 50% of the total charging capacity of the vehicle.

3.2 Supply-side: Power System Model

As one of the primary interests of this work is the compensation for the variability of wind generation injected into the grid, a model to simulate wind generation is necessary. This section introduces the modeling framework for wind energy generation and the basis for calculation of wind generation from meteorological data.

3.2.1 Wind Energy Generation

Modern wind turbines are extremely complex machines, extracting energy from the wind that passes over the turbines blades, producing lift which spins the turbine blades and in turn an induction generator to generate electricity. Due to the large number of components, and relative complexity of the wind generation system, it is generally preferable to develop a simplified transfer function between wind speed input and power output [7].

In its simplest form, the transfer function is defined by a conversion from wind speed to mechanical power imparted to the turbine hub, and a second conversion from the mechanical power imparted to the turbine hub into useful electrical power. A quasi-steady state function defining the mechanical power imparted to the wind turbine P_m as a function of wind speed u_w is given by [53]:

$$\boldsymbol{P_m = \frac{1}{8} C_p(\lambda[k], \beta[k]) \rho \pi D^2 u_w[k]^3} \qquad \textbf{(3.12)}$$

Where D is the rotor diameter, ρ is the air density, and C_p is the turbines coefficient of performance as a function of tip-speed ratio λ and blade pitch angle β. A valid approximation of C_p data, as used in previous works [7], [54], is the relation shown in Equation.

$$C_p[k] = \begin{cases} 0 & u_w < u_{ci} \\ C_{p,m}\left[1 - F_1\left(\frac{u_m}{u_w[k]} - 1\right)^2 - F_2\left(\frac{u_m}{u_w[k]} - 1\right)^3\right] & u_{ci} \le u_w[k] \le u_r \\ C_{p,r}\left(\frac{u_r}{u_w[k]}\right)^3 & u_r \le u_w[k] \le u_{co} \\ 0 & u_w[k] > u_{co} \end{cases} \quad (3.13)$$

Where the turbine cut-in speed (u_{ci}) is the speed at which the turbine begins to generate power, and the turbine cut-out speed (u_{co}) is the speed at which the turbine furls and ceases to generate power. $C_{p,m}$ is the maximum turbine coefficient of performance, defined at the wind speed u_m. The turbine rated speed, u_r, is the speed at which $C_{p,r}$ is defined by the manufacturer. The coefficients F_1 and F_2 are derived from the boundary conditions, namely $C_p = 0$ at $u_w = u_{ci}$ and $C_p = C_r$ at $u_w = u_r$.

As in previous work by Parkinson, it is assumed that a gearbox with S stages is implemented in the transmission of mechanical power to the electrical generator. Consequently, the mechanical power available to the generator is further reduced by the efficiency of the gearbox $\eta_g[k]$ according to equation [55]. The piecewise equation is necessary to ensure that the gearbox efficiency remains positive throughout the operating regime of the wind turbine.

$$\eta_g[k] = \begin{cases} 0.1 & P_m[k] \le \frac{SP_{rt}}{90} \\ 1 - \frac{0.01SP_{rt}}{P_m[k]} & otherwise \end{cases} \quad (3.14)$$

Where P_{rt} is the rated power of the turbine at the rated wind speed, u_r. Additional electrical inefficiencies are not explicitly modeled, but are accounted for via the inclusion of an additional electrical efficiency term η_e in the determination of electrical power provided to the grid according to equation [7].

$$P_W[k] = \eta_e \eta_g[k] P_m[k] \quad (3.15)$$

The input parameters used throughout this thesis for the wind generation model are summarized in

Table 3.3, and are specified to represent a generic 1.5 MW system [7].

Table 3.3 - Parameters implemented in the wind energy system model [7].

Parameter	Description	Value
P_{rt}	Rated power of the turbine	1.5 MW
D	Rotor diameter	82.5 m
u_{ci}	Cut-in wind speed	4 m/s
u_{co}	Cut-out wind speed	26 m/s
u_r	Rated wind speed	12 m/s
$C_{p,r}$	Rated coefficient of performance	0.250
$C_{p,m}$	Maximum coefficient of performance	0.300
u_m	Wind speed at $C_{p,m}$	7 m/s
S	Number of stages in the gearbox	3
η_e	Efficiency of the electrical components	0.95

Sample wind generation data is shown in Figure 3.4 based on NREL 80 m metrological tower wind data for a one-day period [56].

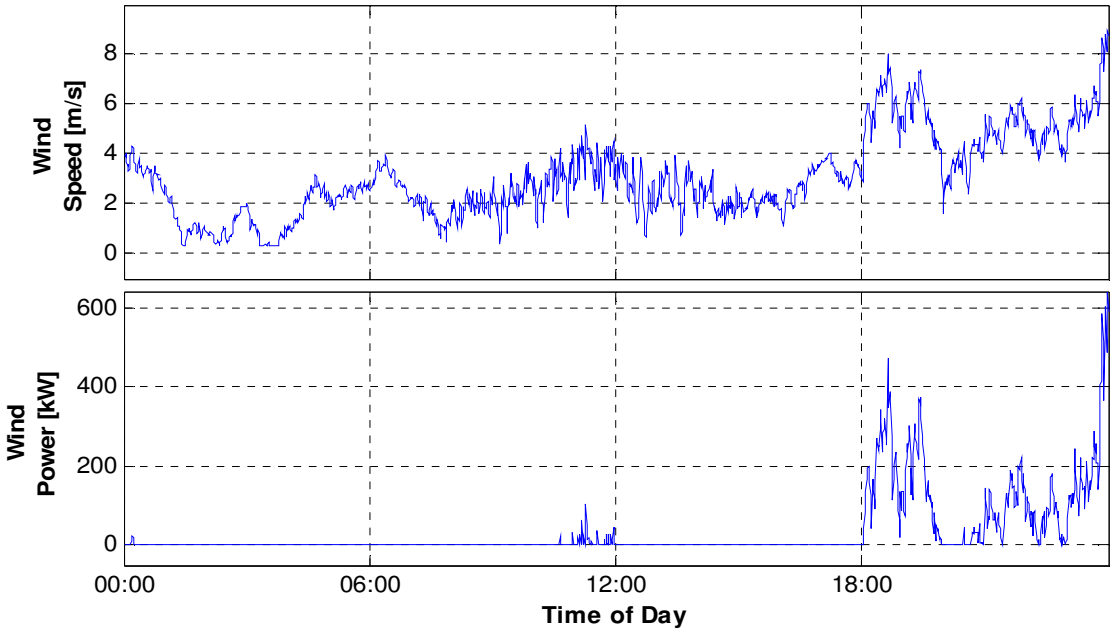

Figure 3.4 - Sample wind speed data (top panel) and resultant model wind generation data (bottom panel).

As one of the primary objectives of this thesis is to reduce the variance in the wind generation injected into the grid, no consideration was given to the effects of multiple turbines or distributed wind generation from multiple locations. Both of these effects generally serve to reduce the variance of wind generation themselves, and thus ignoring them represents a worst-case scenario.

3.3 Selecting the Simulation Time-step

The complete system model, incorporating each component model, requires the ability to capture the dynamics of the load models and wind generation profile, while preserving the accuracy of the system simulations. As in previous works on demand response [7], [8], a one-minute sampling time (T = 1 min) provides sufficient accuracy while permitting transient population dynamics to dissipate. This time-step also permits participation in ancillary service markets such as regulating reserve; services that generally take place on intervals of 5 to 15 minutes [7], [20]. Further, a smaller sampling time could introduce error, as it has been shown that below 1 minute generation does not exactly follow the load [48].

In addition, the 1 minute time step also permits loads to freely enter into and leave the load community – this is particularly important for PEV charging, as users can freely leave the demand response population with minimal impact on overall system performance [7]. Further, the device level controller may not be compatible with longer simulation time-steps and aliasing errors could arise. For these reasons, a 1 minute time-step was selected for all simulations in this thesis.

4 Demand Response Algorithms

The algorithms presented in section 2.5 are now adapted to account for limited reporting of device-state information by a subset of the total participating population of loads in the DR program. The underlying hysteresis control structure is unchanged, however the system response must be calculated based on a limited number of devices reporting device-state information.

4.1 Accounting for Limited Knowledge of Load States

When only a subset of the total participating population is reporting device-state information, the determination of the population capacity factor, and resultant system response must be modified from the algorithms presented in section 2.5. The capacity factor under these limited information scenarios must be determined from only the reporting loads, according to equation (4.1):

$$\boldsymbol{\Phi_{limited}[u_s, k+1]} = \sum_{-\infty}^{u_s+\epsilon_-} \boldsymbol{\phi_{0,r}[\epsilon, k]} + \sum_{-\infty}^{u_s+\epsilon_+} \boldsymbol{\phi_{1,r}[\epsilon, k]} \tag{4.1}$$

The capacity factor determined from device-state information of the reporting loads is then multiplied by the total capacity of the population, including loads that are participating in the DR program but do not report state-information. The resultant response of the system can be determined by equation (4.2):

$$\boldsymbol{P_{cap}[k+1]\Phi_{limited}[u_s, k+1]} = \boldsymbol{P_{cap}[k+1]} \sum_{-\infty}^{u_s+\epsilon_-} \boldsymbol{\phi_{0,r}[\epsilon, k]} + \sum_{-\infty}^{u_s+\epsilon_+} \boldsymbol{\phi_{1,r}[\epsilon, k]} \tag{4.2}$$

The underlying assumption with this control algorithm is that the sampled subset of the total population is representative of the whole population. The VGM limits under limited knowledge scenarios must also be calculated based on the subset of the population reporting device-state information, according to equation (4.3):

$$\begin{aligned} P_{min}[k+1] &= \Phi_{limited}[u_{min}, k+1] P_{cap}[k+1] \\ P_{max}[k+1] &= \Phi_{limited}[u_{max}, k+1] P_{cap}[k+1] \end{aligned} \tag{4.3}$$

These calculations once again rely on the assumption that the sampled subset of loads reporting device-state information is representative of the total population. Further refinement of this control algorithm under limited device-state information are possible by sampling the actual population response and comparing it with the expected response based on equation (4.3). In this manner, a correction factor could be applied to subsequent time-step calculations to reduce the error between anticipated and actual DR population response.

4.2 Control Performance Metrics

The power tracking performance at each one-minute time step was tracked throughout simulations to determine controller performance. To ensure consistent results across all scenarios tested, the systems were initialized at approximately steady state conditions. Two metrics were used in the evaluation of system performance: 1) The root mean squared power tracking error, and 2) The load flexibility and under-utilization factor. These evaluation criteria are explained in detail below.

4.2.1 RMS Error %

The Root mean squared power tracking error (RMSE) is calculated for the duration of the simulation under consideration according to equation (4.4):

$$\boldsymbol{RMSE} = \sqrt{\frac{\sum_{k=1}^{K}(\boldsymbol{P_{actual}} - \boldsymbol{P_{target}})^2}{\boldsymbol{K}}} \tag{4.4}$$

The RMSE is then normalized with respect to the steady state power consumption of the population as shown below

$$\boldsymbol{NRMSE} = \frac{\boldsymbol{RMSE}}{\boldsymbol{mean(P_0)}} \tag{4.5}$$

This metric allows the comparison of various scenarios relative to a standard baseline, and has been used in previous demand response work as a performance criteria [8].

4.2.2 Load Flexibility/Under-Utilization Factor

In addition to the power tracking performance of the system, it is important to determine the load community flexibility and the un-utilized capacity at each time step. Load flexibility is calculated according to equation (4.6), and is analogous to the generator ramp rate of conventional generation resources [7]. Due to the nature of the load community, the load flexibility or ramp-rate is essentially equivalent to the available capacity of the system.

$$\boldsymbol{\mathcal{F}^{(p)}[k] = P_{max}^{(p)}[k] - P_{min}^{(p)}[k]} \quad \textbf{(4.6)}$$

In addition, a measure of the available excess capacity available in each load community for each time step was also calculated. Both up- and down-regulation capacity are evaluated separately, resulting in two under-utilization factors for each time-step. These values are calculated according to equation:

$$\begin{matrix} \boldsymbol{\varphi_{down}[k]} \\ \boldsymbol{\varphi_{up}[k]} \end{matrix} = \begin{matrix} \mathbf{min}((\boldsymbol{P_{max}[k] - P_0[k]}), (\boldsymbol{P_{max}[k] - P_{actual}[k]})) \\ \mathbf{min}((\boldsymbol{P_0[k] - P_{min}[k]}), (\boldsymbol{P_{actual}[k] - P_{min}[k]})) \end{matrix} \quad \textbf{(4.7)}$$

where P_{actual} is the measured power dispatched from the load community for each time step, P_0 is the steady-state power required by the load community, P_{min} is the minimum feasible target power of the load community, and P_{max} the maximum feasible target power of the load community. The minimization operator ensures that actual dispatched capacity is not considered part of the un-utilized capacity available. It is important to note that due to the dynamic nature of the simulations, usage of the un-utilized capacity from one time step will inherently affect the load community for subsequent load steps – however it is a valid measurement of the utilization of the load for offline review. Finally, the total energy dispatched from each VGM population is determined according to:

$$\boldsymbol{E_D^{(p)} = \sum_{k=1}^{N_k} \left|\Delta P^{(p)}[k]\right| T} \quad \textbf{(4.8)}$$

Where up- and down-regulation dispatched are considered equivalent contributions to total energy dispatched by a VGM model.

4.3 Model Input Data

The validity of model input data can greatly influence the results of simulations, thus real world historical datasets relevant to the proposed simulation scenarios were employed. As in previous work [7], the recruited load communities are intended to be representative of a suburban or rural community connected to a single distribution system, or approximately 2000 customers [58]. For the purposes of this thesis, it was assumed that initial populations of 1500 heat pumps and 1500 PEVs could be recruited from this community [7].

To ensure a realistic representation of the loads, populations were intentionally generated to be heterogeneous – this will ensure that the device diversity expected in typical communities is represented. This heterogeneity is achieved by selecting normally distributed values for the individual component models based on representative data for each of the populations under consideration.

4.3.1 Environmental Data - Air Temperature & Wind Speed

Outdoor air temperature and wind speed data were obtained from the National Renewable Energy Laboratory (NREL) database. Specifically, data was obtained from the National Wind Technology Centre M2 Tower, located about 11 km west of Broomfield, and 8 km south of Boulder, Colorado (Latitude: 39° 54' 38.34" North; Longitude: 105° 14' 5.28" West; Elevation: 1855 meters AMSL).

Air temperature measurements are taken at 2m elevation, while wind speed measurements are taken at 80 m elevation. Sample air temperature and wind speed data are shown in Figure 4.1, representing a 24 hour period beginning August 1, 2014 [56].

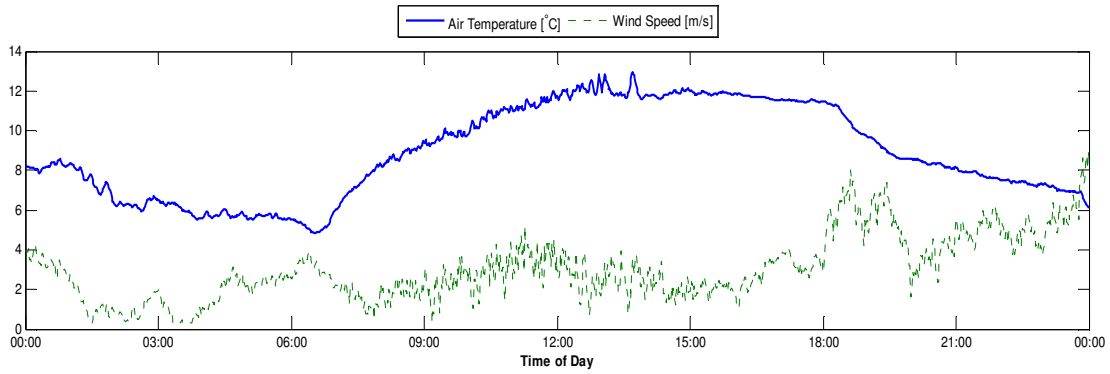

Figure 4.1 - Representative outdoor air temperature and wind speed data from NWTC M2 tower.

In this thesis environmental datasets were selected for the period of October 2013, as this represents a moderate heating demand on the heat pumps, without the requirement to also model cooling loads. During periods of cooler weather, home air temperatures will traverse the deadband region more rapidly than during periods of warmer weather, resulting in greater availability to participate in the demand response program.

4.3.2 Thermodynamic Data - Heat Pump Sizing and ETP Values

For the purposes of simulations in this thesis, parameters used in the ETP model were selected to represent typical single-family homes in the Pacific Northwest. While work is currently ongoing to determine specific ETP parameters to represent a wide variety of buildings [47], there are a number of works that employ the ETP model to represent average homes in the Pacific Northwest [7], [46], and [59].

The ETP model parameters utilized throughout this thesis are summarized in Table 4.1 [59].

Table 4.1 - ETP Model Input Parameters.

Parameter	Description	Value
C	Average thermal capacitance	10 kWh/°C
C_m	Indoor contents thermal mass	75% of C
C_a	Indoor air thermal mass	25% of C
R_{ma}	Indoor heat transfer resistance	0.5°C/kW
R_{ao}	Envelope thermal resistance	2°C/kW
$\dot{q_{fan}}$	Heating power of fan	500 W
θ_s	Temperature set point	20°C
δ	Temperature deadband width	1°C
T	Sampling time interval	1 minute
σ	Noise standard deviation	0.01°C $s^{-1/2}$
σ_p	Standard deviation of lognormal distributions as a fraction of the mean value, for R, C, and P, unless noted otherwise	0.2

Load community populations were then derived from this data by selecting lognormal distributed values from this data, resulting in a homogenous load community as shown in Figure 4.2. Lognormal distributions were chosen primarily to ensure that all parameters remain positive Figure 4.2.

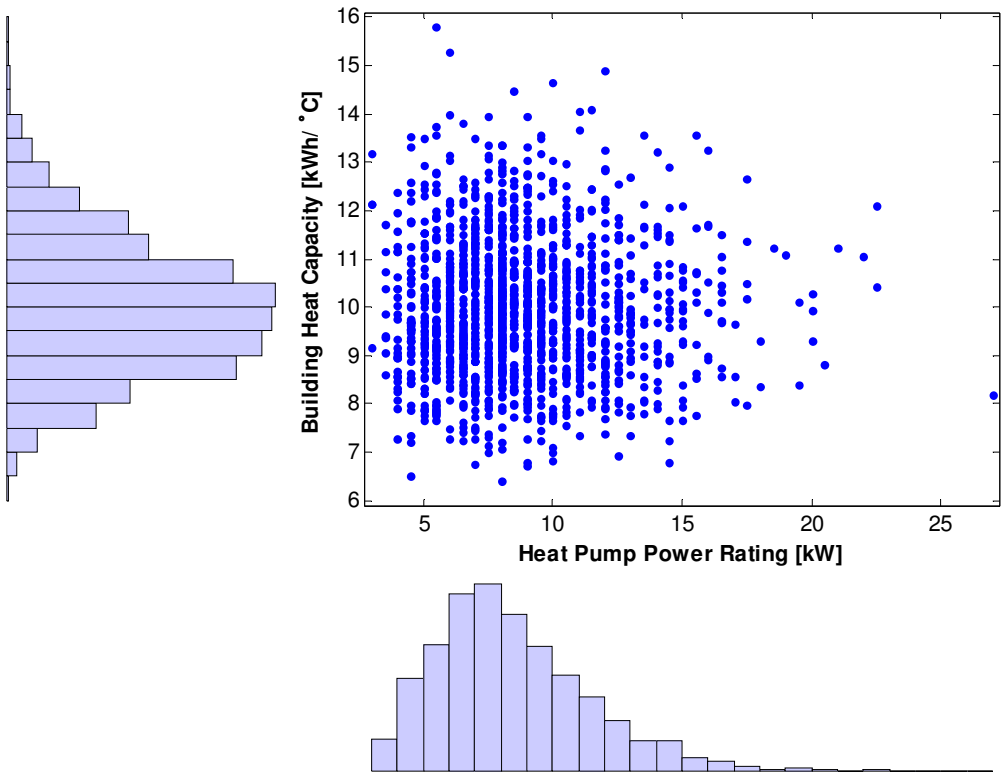

Figure 4.2 - Scatterplot showing selected ETP parameters for a population of 1500 heat pumps.

4.3.3 PEV Data - Vehicle Sizing & Charging Schedules

Previous work incorporating Plug-in Electric Vehicle (PEV) charging loads have generally relied upon estimates of charging schedules and parameters [7]. To increase the accuracy of the PEV load community, results from a survey conducted by SFU of personal driving habits and PEV integration were used to create representative load communities. Survey data included detailed driving parameters of 1754 individuals across Canada, with 538 respondents from BC [52]. Based on this survey data, it was possible to derive the distributions of the parameters required for the PEV charging models employed in this thesis – Specifically the charging start time, charging duration, and required charge

capacity of the vehicle, as summarized in Table 4.2. The rated power of chargers was specified such that the population had an average value of 5 kW, with a standard deviation of 0.5 kW, which are representative of widely available Level 1 chargers.

Table 4.2 - PEV Charging Model Input Parameter Distribution Data

Parameter	Description	Average Value	Standard Deviation
Tstart	Charging start time	17:10 hrs.	235 minutes
Ts	Desired time to accumulate Ec	1018 minutes	313 minutes
Pr	Rated power of charger	5 kW	0.5 kW
Ec	Desired charging capacity	11.3 kWh	2 kWh

Statistical analysis of the survey data showed that the correlation coefficients among charging start time, charging duration, and required charge capacity were all less than 0.1, indicating weak- or no-correlation. As a result, populations of plug-in electric vehicles were generated by selecting random values from these normal distributions. The distribution of charging start and end times from a sample population of 1500 Plug-in electric vehicles is shown in Figure 4.3.

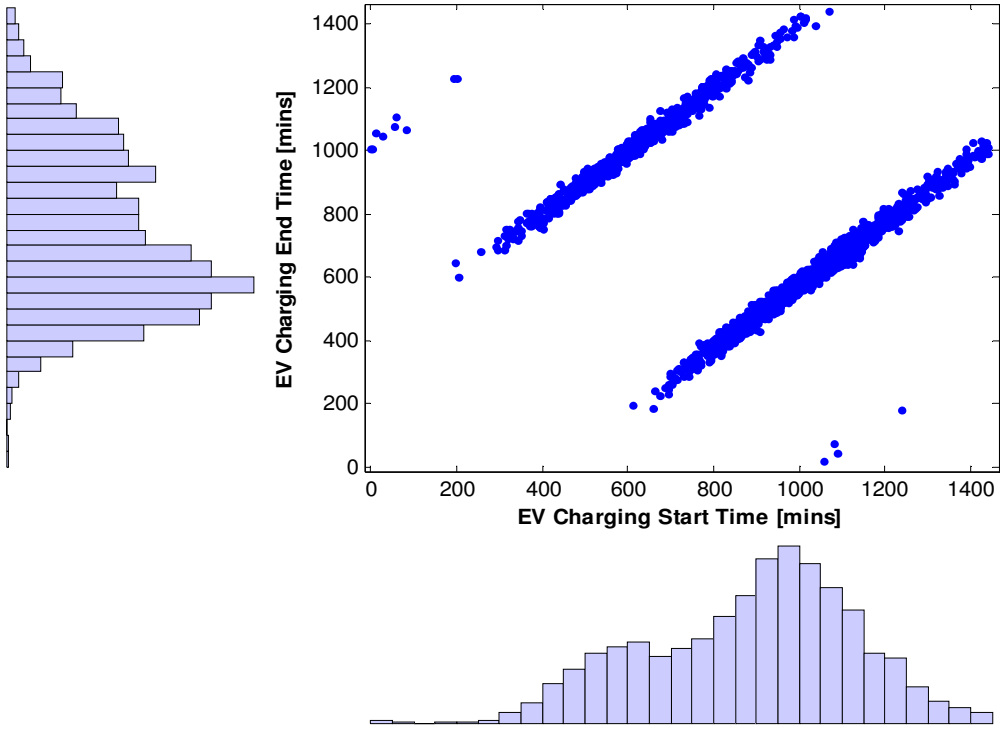

Figure 4.3 - Scatterplot showing PEV charging start and end times.

It is evident from Figure 4.3 that there are two predominant charging windows – the daytime charging window, indicated by the upper diagonal cluster of points, and overnight charging, as indicated by the lower diagonal cluster of points. Further, the availability of daytime charging access was included in the survey data, which was extrapolated to determine the proportion of the population that would have access to daytime charging as shown in Figure 4.4 [52].

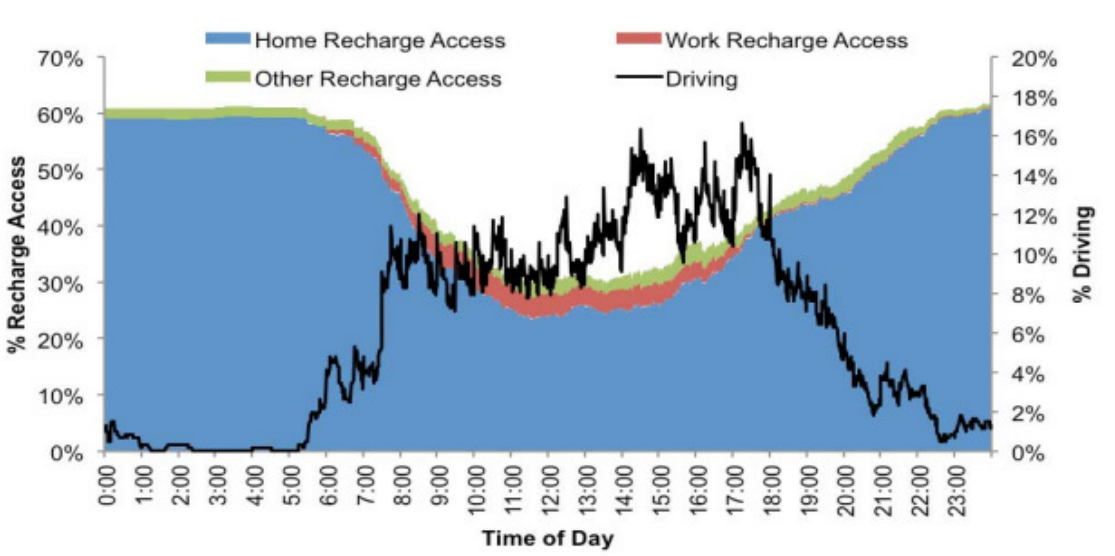

Figure 4.4 - Recharge access by time of day (BC only, n=528, 3-day driving diary) [52].

Approximately 30% of survey respondents had some form of access to charging stations throughout the day, which forms the basis for the percentage of individual loads permitted daytime charging in simulations throughout this thesis.

4.3.4 Target Trajectory

The control algorithms implemented in this thesis are designed to dispatch the participating load communities to meet an externally specified target trajectory provided to the load aggregator. However, if the specified target trajectory exceeds the capabilities of the participating load communities, the target trajectory will be truncated to achieve the largest response possible given the current state of the load communities according to equation (4.9):

$$\boldsymbol{P_T} = \begin{cases} \boldsymbol{P_{min}} & \boldsymbol{P_T < P_{min}} \\ \boldsymbol{P_{max}} & \boldsymbol{P_T > P_{max}} \\ \boldsymbol{P_T} & \boldsymbol{else} \end{cases} \quad \textbf{(4.9)}$$

Where P_{min} and P_{max} are determined based on the maximum permitted control signal magnitude $\delta/4$, previously defined in section 2.5.1.

In scenarios with limited knowledge, however, the value of the capacity factor is calculated based only on the reporting loads. The population is split into two categories: reporting loads (inactive-state, $\phi_{0,r}$ and active-state $\phi_{1,r}$), and participating loads. Under these limited knowledge scenarios, the calculation of P_{cap} is the same as the full knowledge scenarios; however the calculation of the capacity factor is based solely on the reporting loads:

$$\boldsymbol{\Phi_{limited}}[\boldsymbol{u_s}, \boldsymbol{k+1}] = \sum_{-\infty}^{u_s+\epsilon_-} \boldsymbol{\phi_{0,r}}[\boldsymbol{\epsilon}, \boldsymbol{k}]\boldsymbol{\Delta\epsilon} + \sum_{-\infty}^{u_s+\epsilon_+} \boldsymbol{\phi_{1,r}}[\boldsymbol{\epsilon}, \boldsymbol{k}]\boldsymbol{\Delta\epsilon}$$

$$P_{max} = P_{cap}[k+1]\Phi_{limited}[\frac{\delta}{4}, k+1] \quad \textbf{(4.10)}$$

$$P_{min} = P_{cap}[k+1]\Phi_{limited}[-\frac{\delta}{4}, k+1]$$

A target trajectory for the participating loads is thus defined as:

$$\boldsymbol{P^*[k]} = \boldsymbol{Target[k]} + \sum_{\boldsymbol{p=1}}^{\boldsymbol{N_p}} \boldsymbol{P_0^{(p)}[k]} \quad \textbf{(4.11)}$$

This aggregate participating load target, P^* must fall within the range of feasible targets

$$\boldsymbol{P_{min} \leq P^* \leq P_{max}} \quad \textbf{(4.12)}$$

If the aggregate participating load target falls outside of this range, the controller truncates the load target to either the maximum of minimum value that can be achieved by the populations.

In this thesis, two target load trajectories are implemented: a regulating reserve dispatch signal from a utility operator, and a self-generating signal to reduce the variability of wind generation from a wind turbine. These target trajectories are described in detail in the following sections.

4.3.4.1 *Regulating Reserve Dispatch Signal*

In order to test the demand response system to provide regulating reserve ancillary services to the power systems operator, a target trajectory was specified based on historical regulating reserve capacity dispatched in the BPA balancing authority area [19], as shown in Figure 4.5.

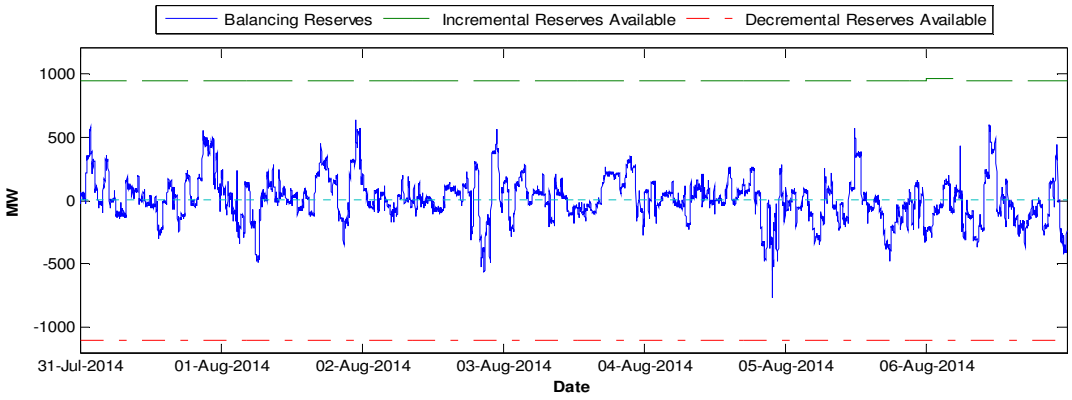

Figure 4.5 - BPA Balancing Reserves Available & Dispatched July 31 - Aug 7, 2014 [19]

The target trajectory was then generated by scaling the balancing reserves dispatched values for a 24-hour simulation period, and inverting the sign to ensure a request for generation results in a decrease in demand. As this portion of the balancing reserves are then served by the demand response program, the resultant balancing reserves required by the balancing area to be supplied from conventional generation resources will be reduced. The frequency distributions of one year's worth of BPA balancing reserves dispatched data is shown below in panel 1 of Figure 4.6, which closely resembles the frequency distribution of the 24-hour simulation period balancing reserves deployed used as a basis for the target trajectory for simulations in this thesis.

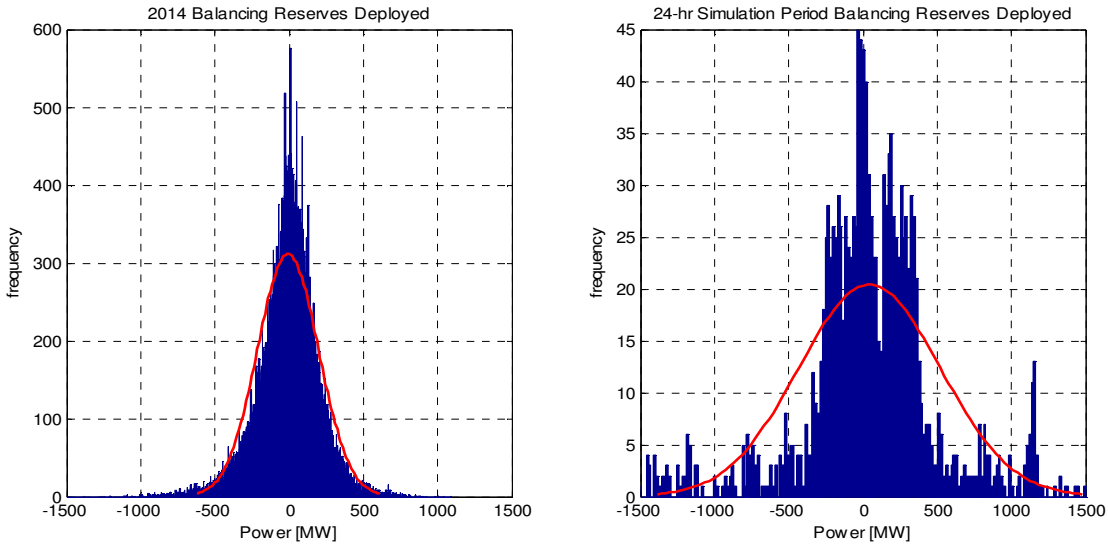

Figure 4.6 - Frequency distribution of BPA balancing reserves dispatched data from 2014 (left panel) and 24-hour simulation period (right panel).

The similarities among the frequency distributions of the data for balancing reserves dispatched in Figure 4.6 shows that the 24-hour simulation window is representative of annual balancing reserves dispatched. The target trajectory was scaled down to 0.5% of the total balancing reserves dispatched in the BPA network, to ensure that it was within the feasible region for populations of 1500 homes and 1500 EVs.

4.3.4.2 Reducing Variability of Wind Generation Target Signal

As described in section 3.2.1, wind energy generation exhibits considerable variability at a one-minute resolution time-step, especially when considering an individual wind turbine or single wind farm. It is possible to utilize demand response programs to modify the demand curve in response to variations in wind generation, thus resulting in a significant reduction in variability to the net power required from the electrical grid. For the purposes of this thesis, a target trajectory to smooth wind generation injections from a single 1.5 MW wind turbine is employed. The target trajectory attempts to the net power injections into the grid according to the 15 minute moving average wind generation profile according to equation (4.13):

$$\boldsymbol{Target}[\boldsymbol{k}+\mathbf{1}] = \boldsymbol{P}_{\boldsymbol{wind},\mathbf{15\,min}\,\boldsymbol{avg}}[\boldsymbol{k}] - \boldsymbol{P}_{\boldsymbol{wind},\boldsymbol{actual}}[\boldsymbol{k}+\mathbf{1}] \qquad \textbf{(4.13)}$$

Where the 15 minute moving average is calculated according to equation (4.14):

$$\boldsymbol{P_{wind,15\,\mathrm{min}\,avg}[k] = \frac{1}{15}\sum_{m=-15}^{0} P_{wind,actual}[k+m]} \qquad \textbf{(4.14)}$$

This target trajectory assumes that the next time-step wind generation is known, however this is not an unreasonable assumption given the accuracy of conventional persistence modeling and advanced meteorological modeling [59]. A target trajectory based on sample wind speed data is shown in Figure 4.7.

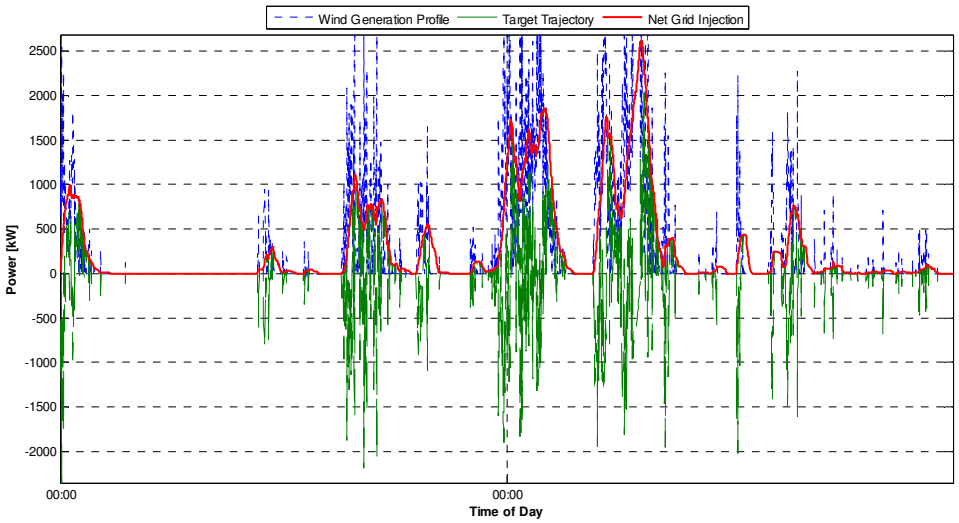

Figure 4.7 - Sample target trajectory and net grid power injections based on wind generation profile from section 3.2.1.

As shown in Figure 4.7, the demand response target will always supply the difference in generation at each time step from the 15 minute moving average, smoothing the net impact of variable generation injected into the grid. Figure 4.8 shows the frequency distribution of wind speed at the NREL meteorological tower [56] for the past year (left panel), and for the 24-hour simulation period under consideration (right panel)

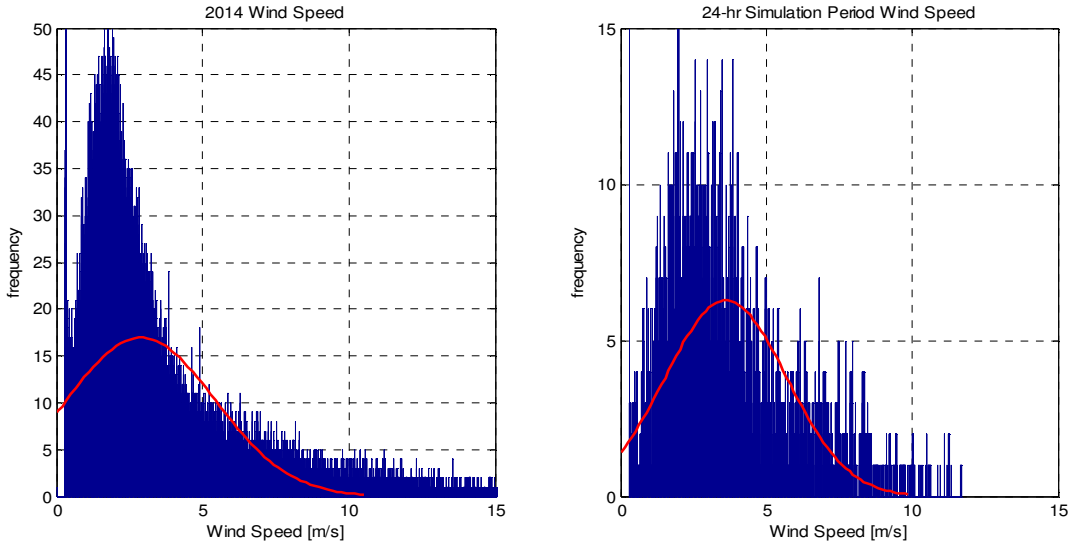

Figure 4.8 - Frequency distribution data for NREL wind speed data from 2014 (left panel) and 24-hour simulation period (right panel).

While seasonal variations will exist with respect to wind speed data and the resultant wind generation injections into the grid, the 24 hour sample period provides a representative sample of the major short-term variability to be expected from a demand response program operating to smooth wind energy generation injections. The target trajectory was specified to simulate smoothing the power injections to the grid from a 3 MW wind turbine to ensure that it always remains in the VGM feasible regions for 1500 Homes and 1500 EVs.

5 Model Results

This section will present simulation results, initial analysis of the VGM population dynamics, and draw conclusions with respect to the observed performance of the proposed demand response system. In all scenarios, simulations were run for a 2-day period (2881 minutes). The first 24-hours (1440 minutes) of the simulation results were discarded to ensure any transient response from initializing the demand response program did not affect the results of the simulations, and all analysis was conducted on the data from the remaining 24-hour simulation period.

5.1 Provision of Wind-Generation Smoothing Services

A second scenario was considered for the demand response system, utilizing the VGMs to smooth wind generation injections into the electrical grid. Historically, increased penetration of wind generation into the electrical grid has necessitated additional dispatchable power capacity to firm-up the variable power injections from wind generation [12]. In the wind-firming scenario, rather than relying on conventional dispatchable generation to firm wind power injections, demand response populations are utilized to adjust demand in real-time in response to variations in wind power generation. In this scenario, the target trajectory is specified according to the procedure indicated in section 4.3.4.2, and shown in Figure 5.1.

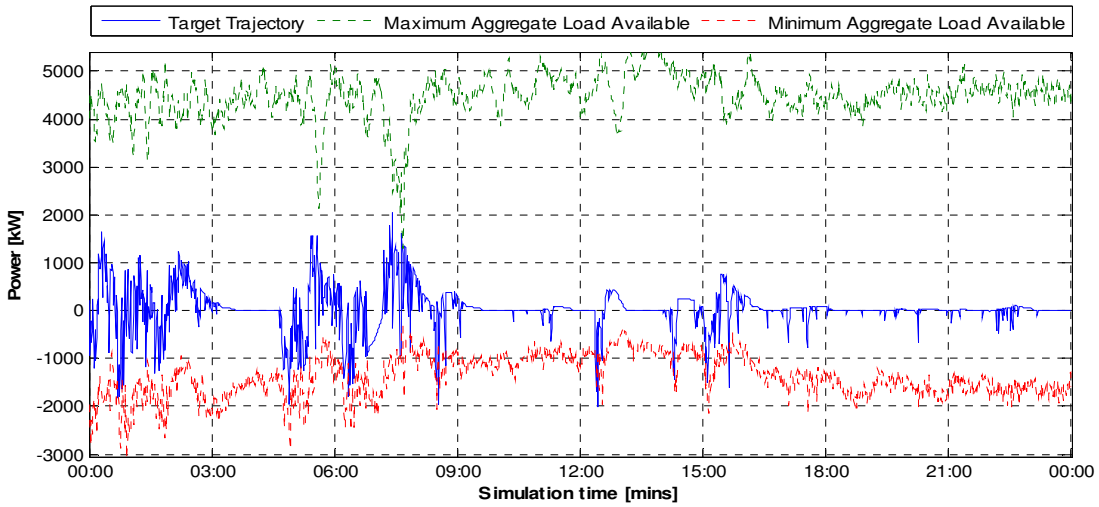

Figure 5.1 - Wind Generation Smoothing Target Trajectory

This target trajectory results in a net injection to the electrical grid equivalent to the 30-minute moving average of the wind generation values, rather than the highly variable real-time wind generation profile shown in Figure 5.2.

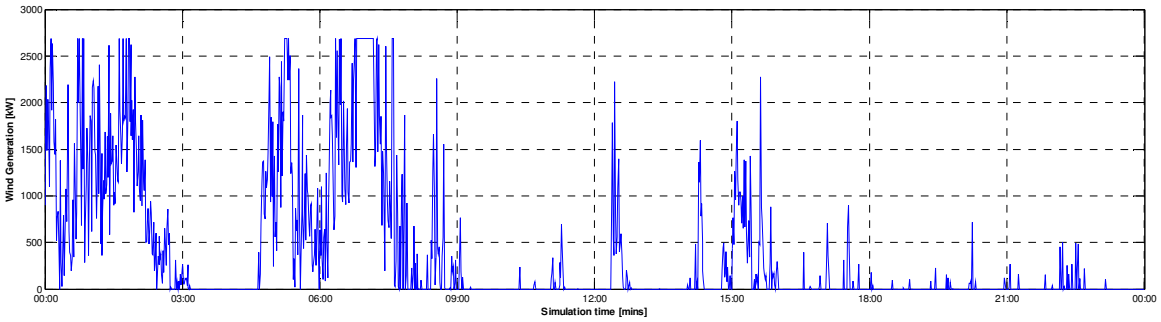

Figure 5.2 - Wind Generation over 24-hour Simulation Period.

As a result, the variability of power injections into the grid are greatly reduced, reducing the requirements for conventional dispatchable generating resources to provide balancing reserves. Once again, 1500 heat pumps and 1500 EVs were selected for this scenario, and the wind farm capacity was scaled such that the target trajectory remains within the feasible region throughout the simulation period, as shown in Figure 5.1.

Again, the resultant VGM response is within 2% of the target trajectory, primarily attributed to discretization of the deadband region and quantized device-level power ratings. The resultant controlled and uncontrolled trajectories of each VGM, and the cumulative population trajectory are shown in Figure 5.3.

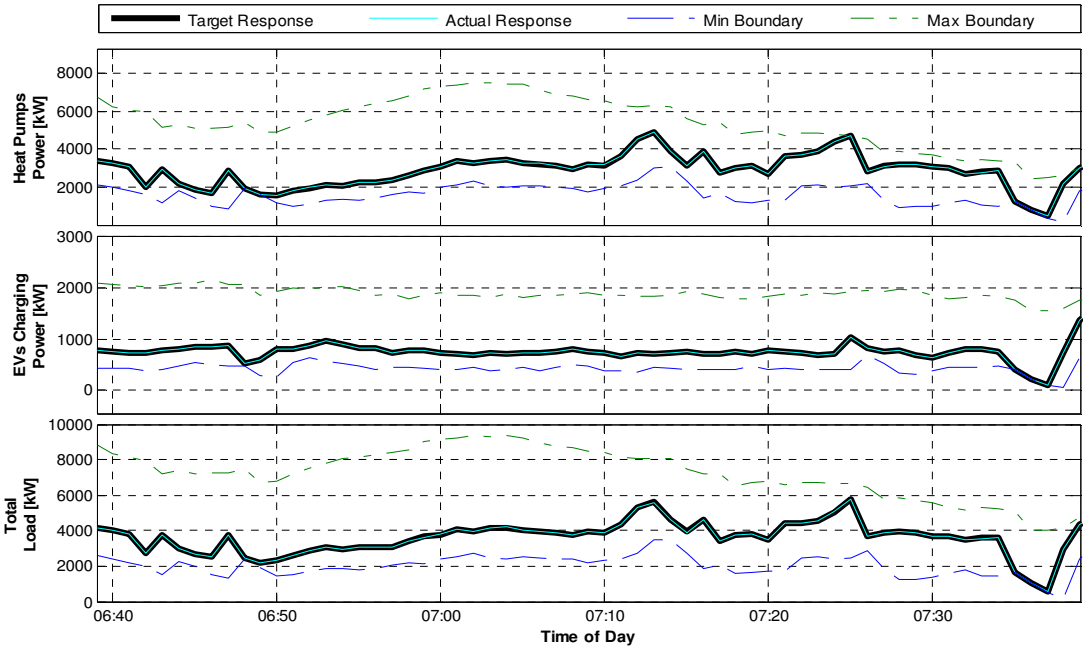

Figure 5.3 - Demand Response System trajectories.

Similarly to the scenario providing ancillary services in the previous section of this thesis, the Heat Pump VGM exhibits greater flexibility, once again owing to the transient nature of EV Charging vehicles connecting to and disconnecting from the system throughout the day. The individual VGM flexibilities and under-utilized capacities are shown in Figure 5.4.

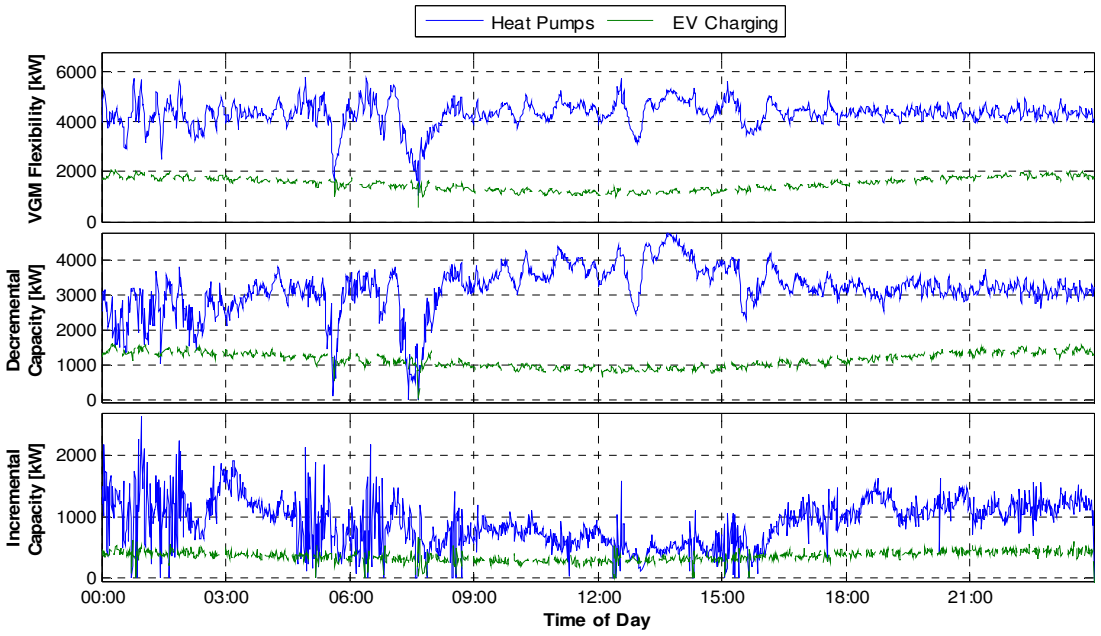

Figure 5.4 - Individual VGM flexibility and under-utilization factors.

Power density distributions for each of the VGMs are also similar under the wind-firming scenario as they are in the regulation reserve scenario, as shown in Figure 5.5.

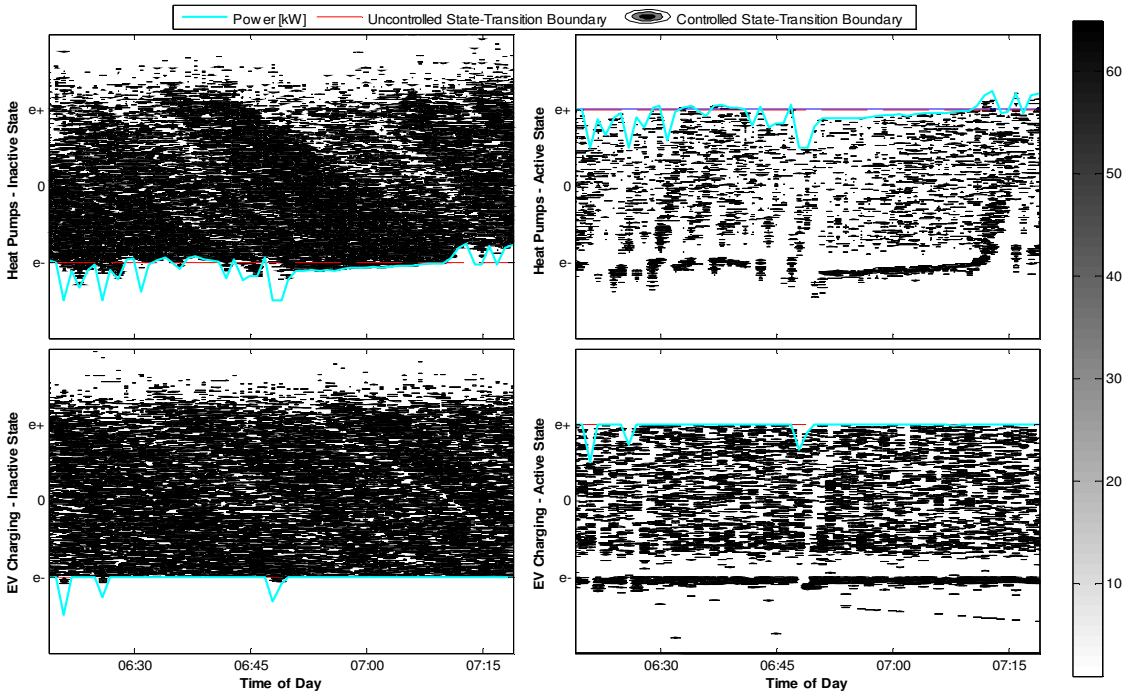

Figure 5.5 - Density plots of VGMs.

Large magnitude control signals result in synchronization of loads within each of the VGMs, however this load synchronization rapidly dissipates naturally throughout the populations due to the heterogeneous populations modeled.

Again, owing to the larger available capacity of the Heat Pump VGM compared to the EV charging VGM, the Heat Pump VGM dispatched almost twice the energy throughout the simulation period, as shown in Table 5.1.

Table 5.1 - Performance of Load Resources Performing Wind Smoothing Services.

Load Type	Dispatched Energy [MWh]	Mean VGM Flexibility [MW]	Mean Control Signal Magnitude [% of u_{max}]	Control Signal Standard Deviation [% of u_{max}]
Heat Pumps	6.04	4.35	0.43	20.49
EV Charging	0.182	1.186	0.68	3.30

The magnitude of the mean control signal for both populations was very small, primarily due to the large variations in wind generation power over short time periods, coupled with extended periods of zero wind generation. As the target trajectory was scaled to ensure it was always within the feasible region of the VGMs, the utilization of the VGMs during non-peak target trajectory periods is rather low. If conventional balancing resources were utilized to cover the large spikes in target trajectory, a much larger amount of energy could be dispatched from the demand response program. It would thus be possible to employ the demand response system to provide additional services concurrently with wind-generation smoothing during the periods of zero or low wind generation.

5.1.1 Limited-knowledge Population Dynamics

In order to test the effects of limited knowledge on the demand response system, and the individual VGM population dynamics, eleven additional scenarios were considered with progressively less device state information. Simulations were conducted with reduced knowledge, ranging from 100% knowledge to 20% knowledge, to determine the effects on overall system response when providing wind generation firming services using the same target trajectory as shown in Figure 5.1. The overall load trajectories of these simulations,

as well as the actual system response under various limited device-state information scenarios are shown in Figure 5.6.

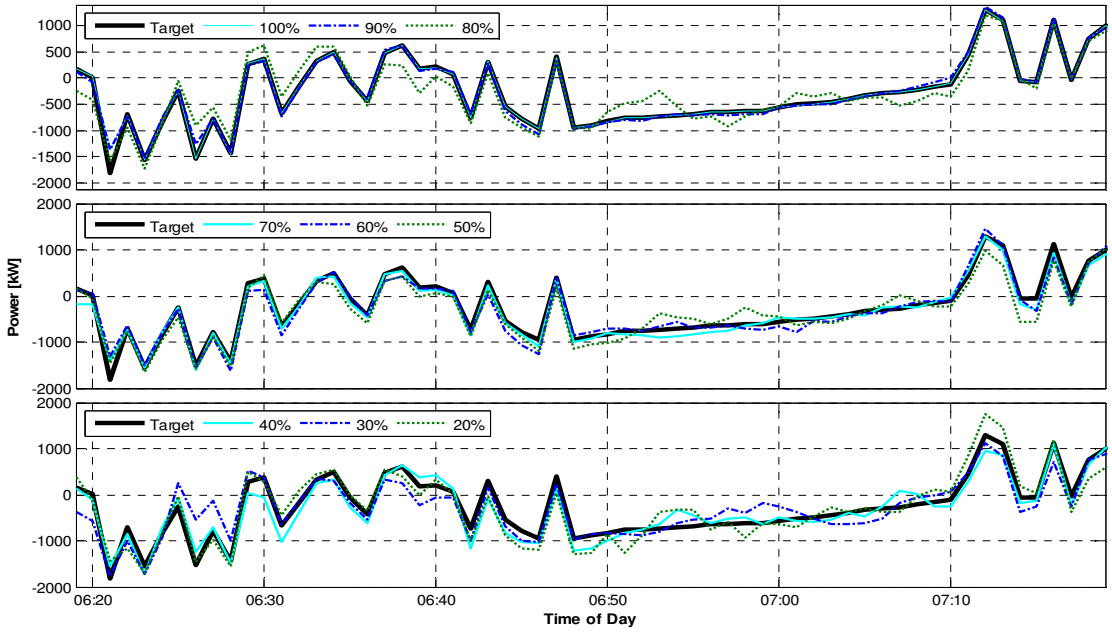

Figure 5.6 - System response and Target trajectory under limited-knowledge simulations.

As shown in Figure 5.7, the error associated with the VGM response increases as device-state information is decreased, as would be expected. However, even at very low state-information levels the normalized root mean squared error associated with the demand response system remains below 10%. Once again, this error is largely attributed to discretization of the deadband region, and quantized device-level power ratings; although the reduced information scenarios amplifies these effects noticeably.

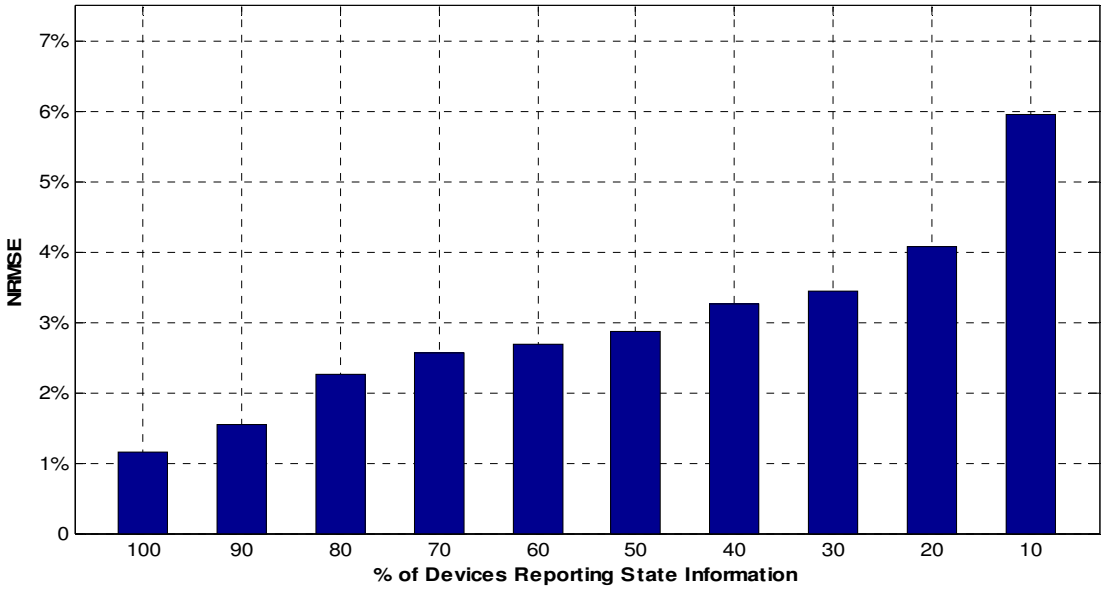

Figure 5.7 - NRMSE associated with varying levels of device-state knowledge for wind-firming target trajectory.

The response of the individual load communities, as well as the feasible regions, are shown in Figure 5.8 for the 100%, 80%, and 50% knowledge scenarios.

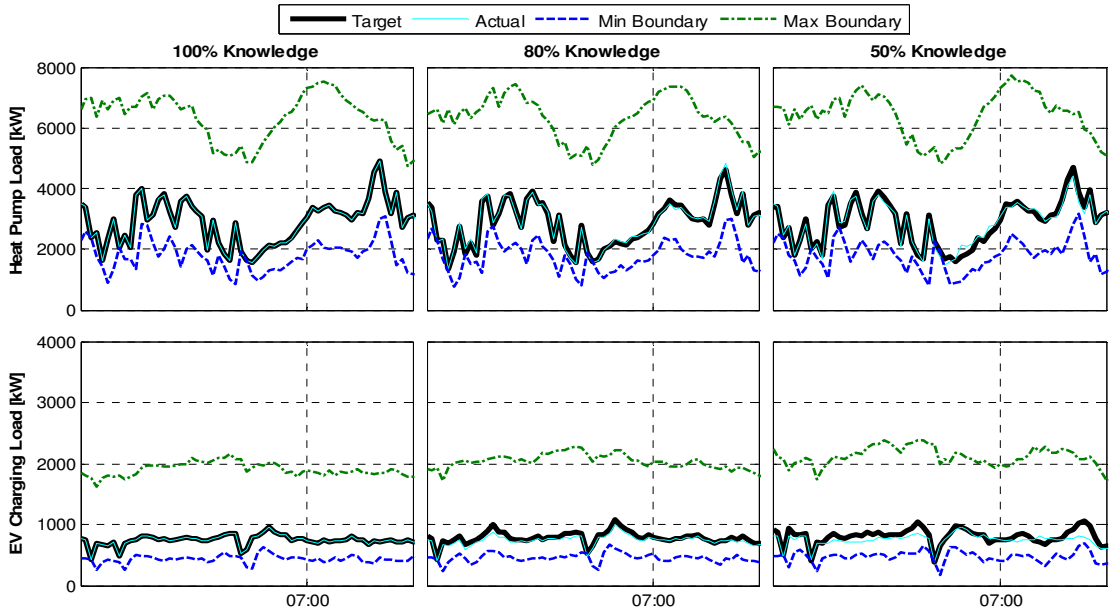

Figure 5.8 - Individual VGM response for 100%, 80%, and 50% knowledge scenarios.

It is apparent from Figure 5.8 that the heat pump VGM provides the most consistent response for all device-state knowledge scenarios, as the individual participating loads of the EV population are once again connecting and disconnecting from the system throughout the day. This additional uncertainty in the EV population results in greater error under limited knowledge scenarios, as shown in Figure 5.9.

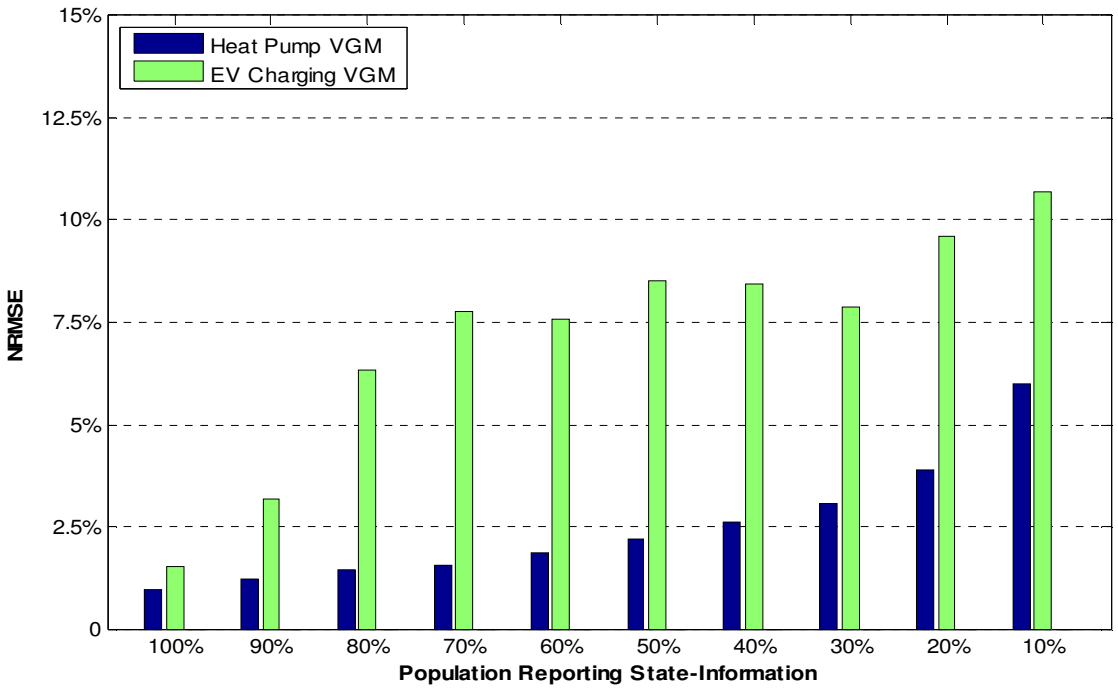

Figure 5.9 - NRMSE associated with individual VGM populations for various knowledge levels.

Once again, the error increases more rapidly for the EV charging VGM due to the transient nature of electric vehicles participating in the DR program. This effect could be minimized by including sensors to detect if an EV is attached to a charging station, particularly for public or workplace charging stations where the privacy concerns would be alleviated by the public nature of the charging stations. This would eliminate the uncertainty associated with EV users plugging into and unplugging from charging stations to utilize their vehicles, bringing the error associated with the VGM closer to that of the heat pump VGM.

5.1.2 Capacity Determination for Wind-Generation Smoothing

The effects of population size on available demand response capacity, and overall energy dispatched when providing wind-generation smoothing services were evaluated by running

simulations of populations ranging in size from 500 devices to 6000 devices. Heterogeneous populations of equal numbers of heat pumps and EV charging loads were paired with iteratively scaled target trajectories to ensure that the populations were never over-dispatched. Simulations of each population size (500, 1000, 1500, 3000, 4500, and 6000) were conducted under 100% knowledge scenarios, and the resultant mean VGM capacities and net energy dispatched was evaluated. Figure 5.10 shows the energy dispatched by the DR program for various population sizes, as well as the mean available capacity of the VGMs of varying sizes.

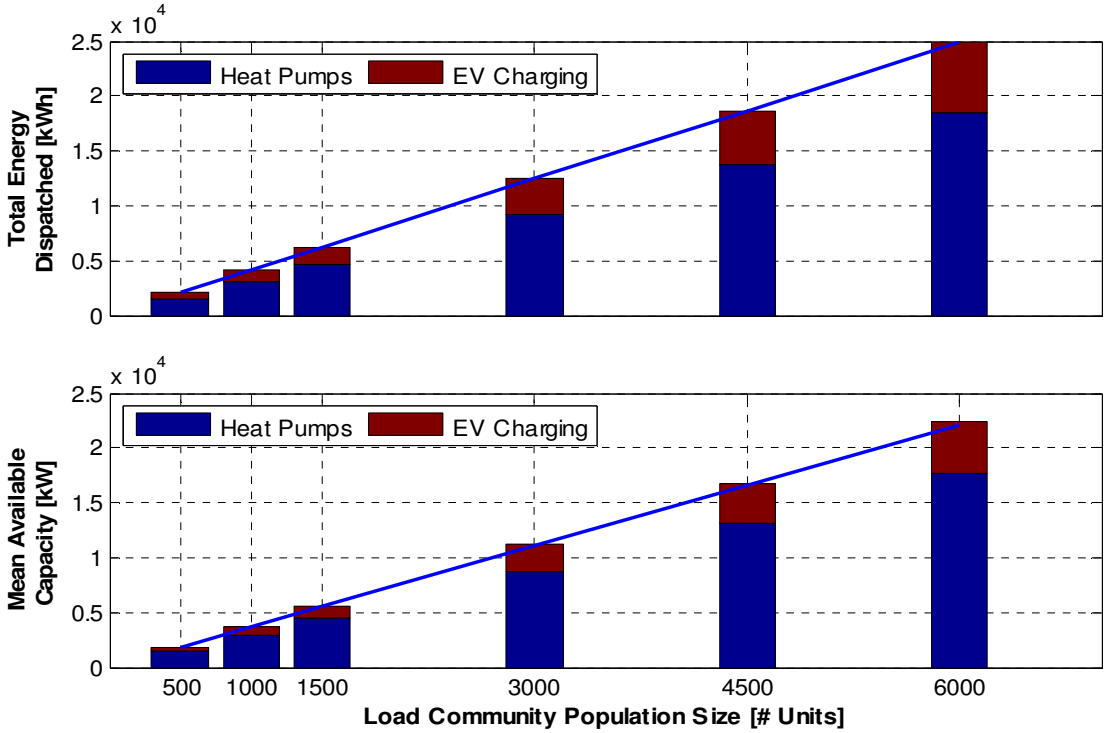

Figure 5.10 - Energy Dispatched by VGMs (top panel) and Mean Available VGM Capacity (bottom panel) for Various Load Community Population Sizes.

As the population size of the VGMs is increased, the dispatched energy from the DR program increases proportionally. In addition, the available mean capacity of the DR program increases proportionally with the population size. Each VGM responds similarly, with the heat pump VGM remaining the largest contribution to the demand response program in these scenarios.

The effects of scaling population sizes on the available mean capacity would be useful for utility systems operators to determine how many responsive loads they would need to recruit to achieve a desired capacity from the DR program. In all scenarios, the mean control signal magnitude and the control signal standard deviation remained within 1% of one another, and within 2% of one another, respectively. This implies that the inconvenience of the DR program on end-user functionality is not significantly affected by VGM population size.

5.2 Provision of Regulating Reserve Ancillary Services

To simulate the provision of balancing reserve ancillary services to a power systems operator, a target trajectory corresponding to the BPA historical balancing reserves dispatch history was created as described in section 4.3.4.1. This target trajectory was then iteratively scaled to a point where it remains entirely within the feasible region of the VGM of home heat pumps and PEV charging, as shown in Figure 5.11. This scaled trajectory represents 0.5% of the total balancing reserves dispatched by the BPA over a 24-hour period [19].

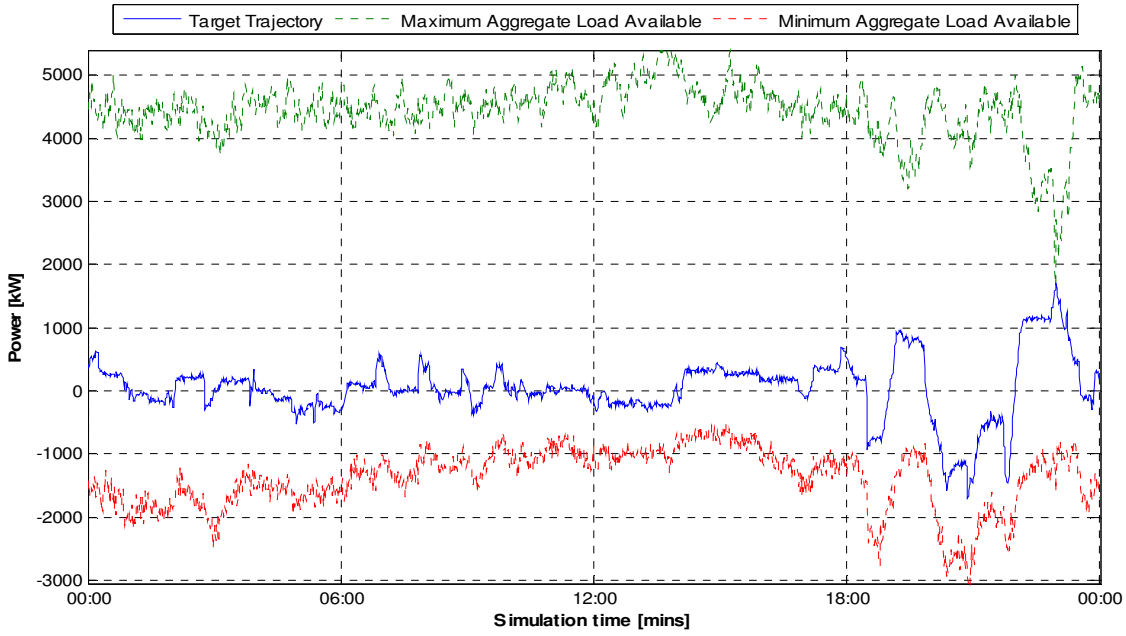

Figure 5.11 - Scaled target trajectory & VGM feasible region boundaries.

Heat pump and PEV charging populations were selected to represent a small suburban or rural community connected to a single distribution system, resulting in populations of 1500 heat pumps and 1500 PEVs [58]. To represent the diversity of real-world populations, heat pump and PEV charging parameters were drawn from normal distributions of parameters as described in the previous sections.

With the model inputs defined, two preliminary scenarios were considered: The first, without any intervention by the demand response system to represent the uncontrolled trajectory of the load populations; and the second with the demand response system applied under the assumption of full device-state knowledge. The resultant load trajectories under both scenarios, as well as the individual VGM responses, are shown in Figure 5.12.

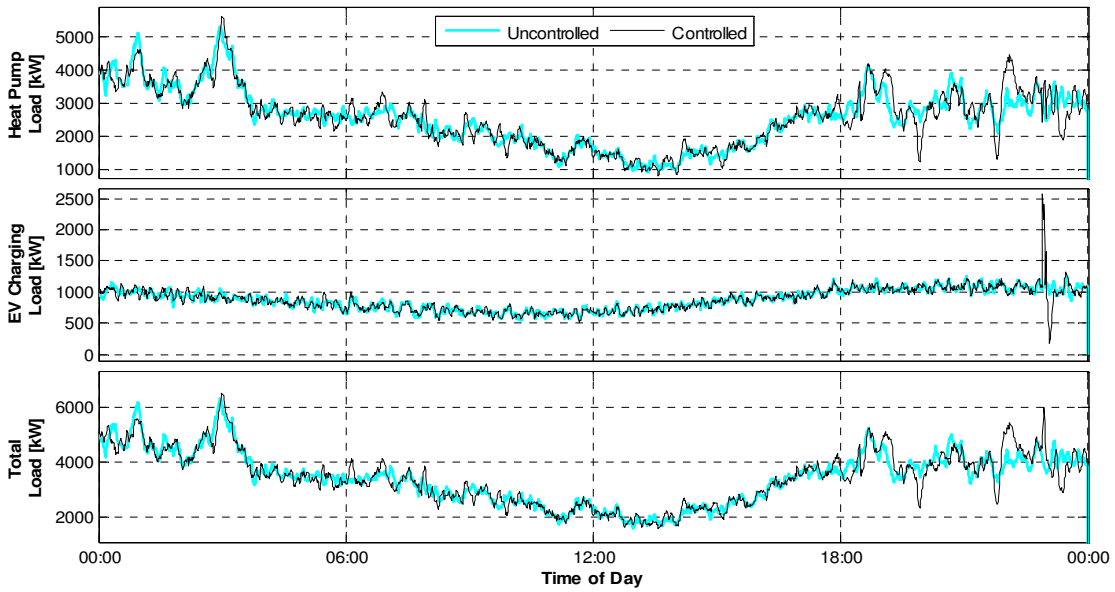

Figure 5.12 - Uncontrolled and Controlled Population Response.

The controlled scenario follows the target trajectory specified, resulting in less than 2% NRMSE throughout the simulation period. The heat pump loads provide greater demand response capacity than the PEV charging loads due to the fact that the heat pumps are available throughout the entire 24 hour period, while PEV charging loads enter and leave the demand response program as they are utilized by owners for transportation. Detailed

plots showing the individual VGM responses, as well as the feasible region, are shown in Figure 5.13

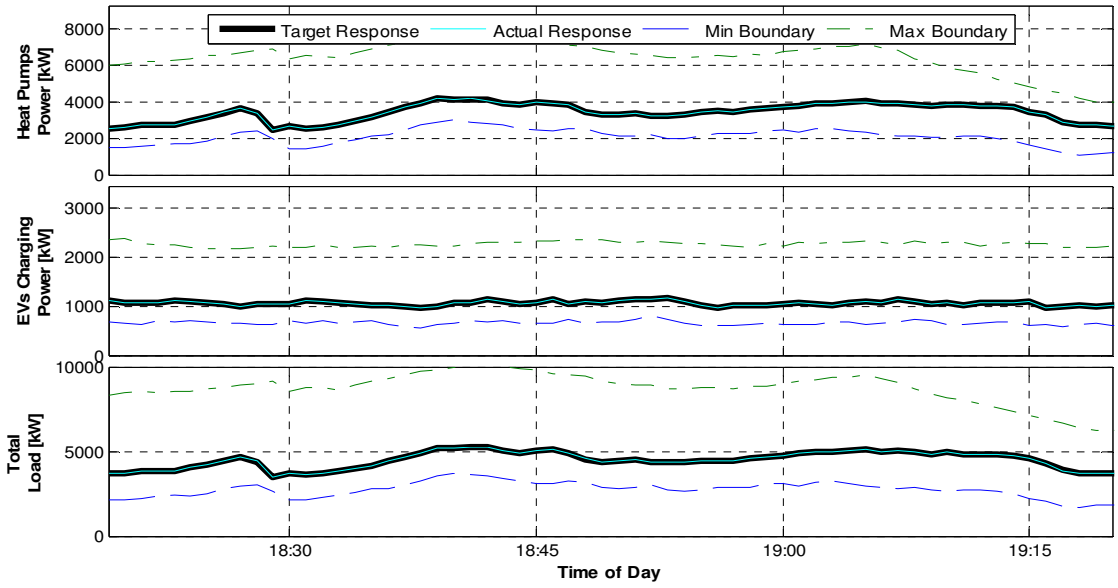

Figure 5.13 - Individual VGM Feasible Regions, Target Trajectory, and Actual Response.

The maximum and minimum boundaries define the largest magnitude response that the VGM is capable of providing to the system at each time step, and changes throughout the simulation period in response to utilization of the demand response resource. As a result, the specified target trajectory must remain within these boundaries throughout the demand response program operation to ensure the desired response from the system is feasible.

The flexibility and the under-utilization factors of the VGMs, as described in section 4.2.2, are shown below in Figure 5.14.

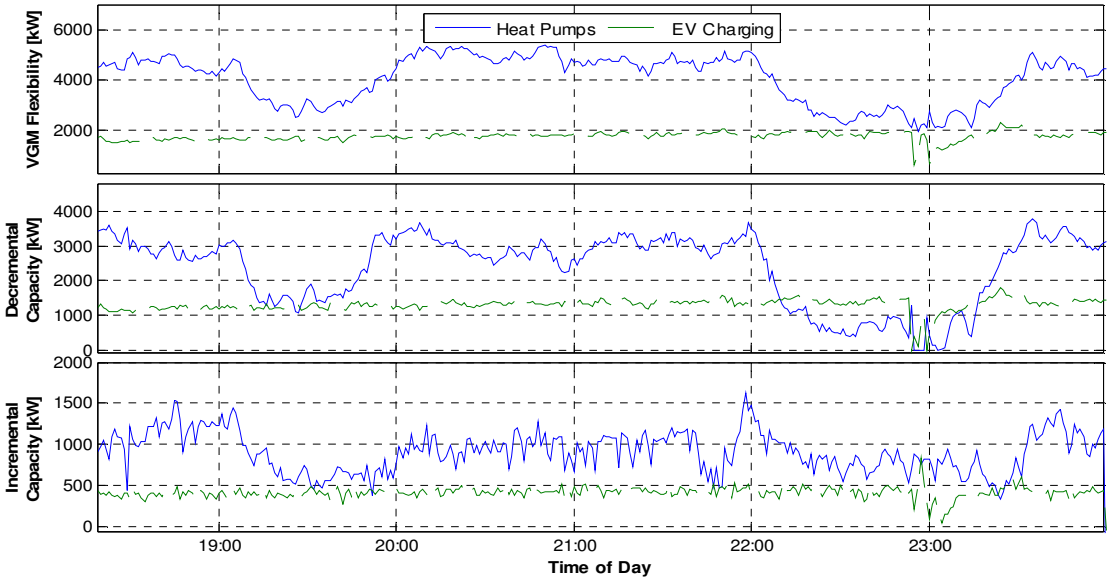

Figure 5.14 - VGM Flexibility and under-utilization factors.

This represents the maximum feasible region within which demand response services are achievable for the VGMs, as well as the effective ramp-rate that each VGM is capable of achieving in the next time-step. It is important to note that the feasible region is constantly evolving in response to the dispatched power from previous time-steps as devices transit the deadband region and replenish the population flexibility. There are a few instances throughout the simulation period where the incremental capacity of the VGMs approaches saturation, however these regions of saturation rapidly replenish when the output demanded of the VGMs is reduced. This can clearly be seen in Figure 5.14 above for the Heat Pump VGM between the hours of 22:30 and 23:30. The resultant power density distributions of all devices within the VGM are shown in Figure 5.15.

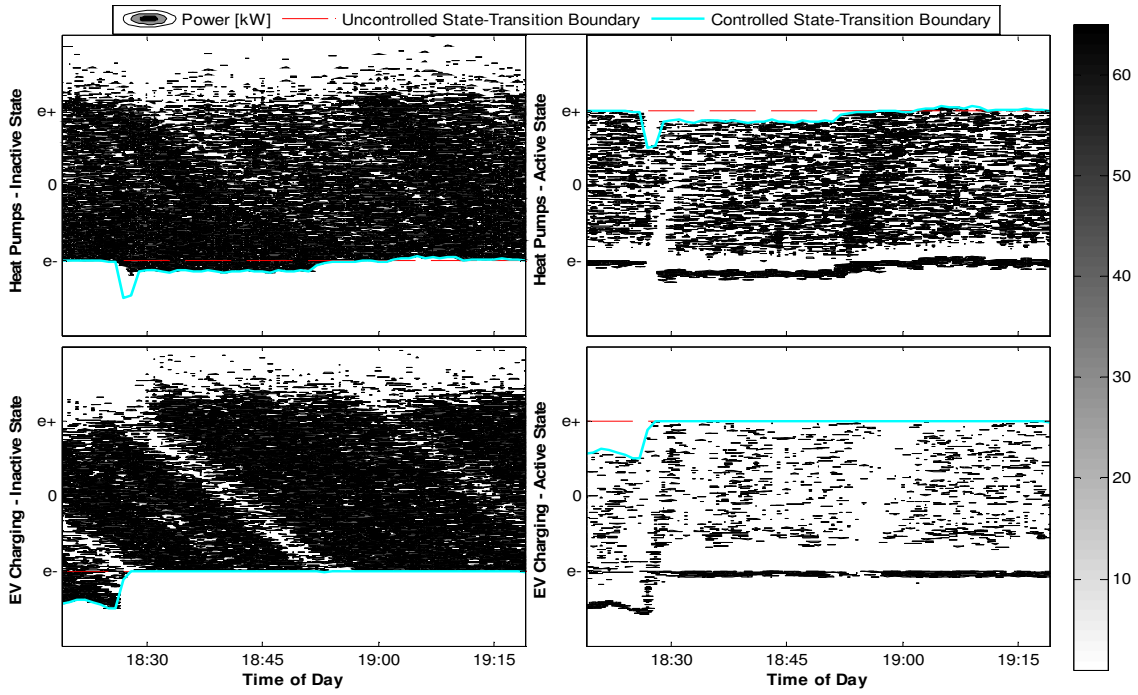

Figure 5.15 - Load Community Power Distributions.

The cumulative power density of units at each individual end-use state is shown over the discretized 2δ-deadband region, as well as both the controlled and uncontrolled state-transition boundaries over the plotted simulation period. Limited state-transition boundary overshoots are observed infrequently throughout the simulation period, and can be attributed to devices in the preceding interval diffusing into the state-transitioning regions, which are then adjusted during the next time-step management operation. Regions where the VGM output nears the feasible region boundary in Figure 5.13 correspond to events in which the control signal lies along its minimal level as defined by equation 4.3. These occurrences of maximal control signal magnitude result in transient device-state synchronization, most clearly visible in the EV Charging –inactive state panel of Figure 5.15 shortly before 18:30 hrs. The EV Charging VGM exhibits greater device synchronization than the Heat Pump VGM, but dissipates quickly as the populations are heterogeneous enough to maintain load diversity.

Both VGMs exhibit a band of device-state synchronization at the lower boundary of the active-state regions. This synchronization is rapidly dissipated due to the heterogeneous populations of devices within each load group, and is the result of the binning of all devices above and below the state-transition boundaries being grouped into the same state-bin at

the limits of the discretization. This aggregation is necessary to maintain user-comfort constraints despite a heterogeneous population, and does not introduce any detrimental system operating effects.

The Heat pump VGM exhibits the greatest flexibility to quickly damp disturbances in state diversity and maintain distribution uniformity. This is further evidenced by the fact that the Heat Pump VGM maintains the greatest flexibility throughout the simulations, as shown in Figure 5.14.

The dispatched power from each VGM population, as well as the mean flexibility of the VGM is presented in Table 5.2.

Table 5.2 - Performance of Load Resources Performing Balancing Services.

Load Type	Dispatched Energy [MWh]	Mean VGM Flexibility [MW]	Mean Control Signal Amplitude [% of u_{max}]	Control Signal Std Dev [% of u_{max}]
Heat Pumps	1.68	4.26	6.4	24.1
EV Charging	0.72	1.18	0.4	24.6

The heat pump population is dispatched for the most energy, while the EVs provide less energy largely due to their dynamic population size as they are connected and disconnected from the VGM throughout the day to be driven. The dispatch algorithms will dispatch both VGM populations based on their total available capacity, and as a result the Heat Pump population generally provides a larger portion of the total energy dispatched in the demand response system. A more aggressive target trajectory would result in greater utilization of the VGM populations, however care must be taken to ensure that the target trajectory remains within the feasible region of each VGM.

5.2.1 Limited-Knowledge Population Dynamics

In order to test the effects of limited knowledge on the demand response system, and the individual VGM population dynamics, eleven additional scenarios were considered with progressively less device state information. Simulations were conducted with reduced knowledge, ranging from 100% knowledge to 20% knowledge, to determine the effects on

overall system response when providing regulating reserve ancillary services using the same target trajectory as shown in Figure 5.11. Figure 5.16 shows the overall load trajectories of these simulations for an increasing portion of the participating loads not reporting device-state information.

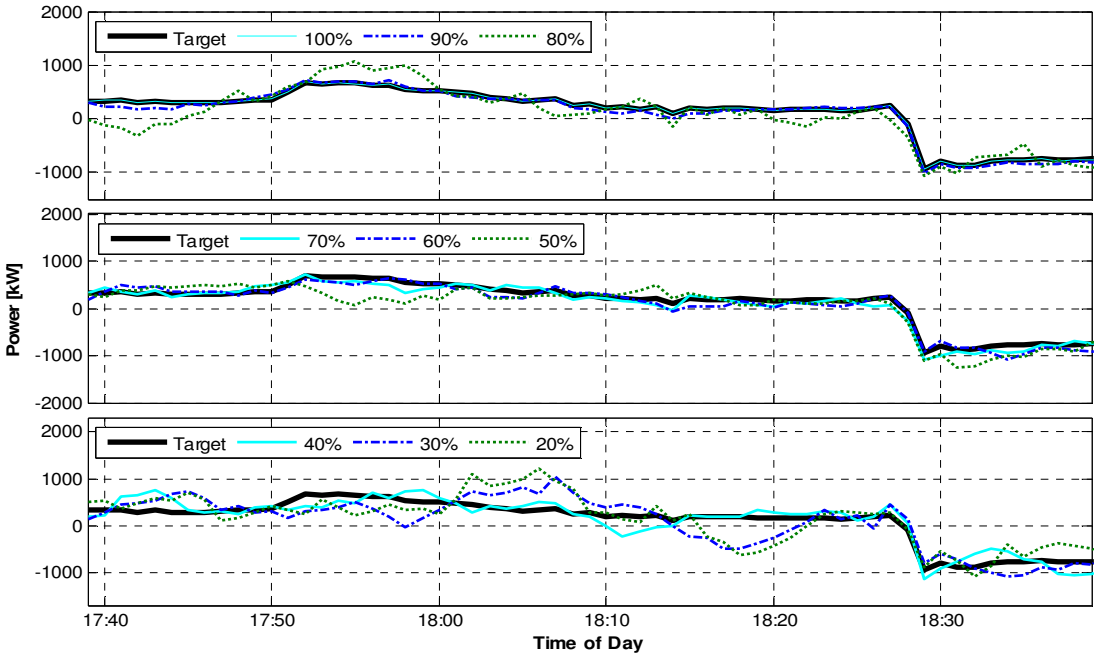

Figure 5.16 – Aggregate system response under limited-knowledge simulations.

As shown, in scenarios with less than full device-state knowledge, the demand response program frequently under- or over-dispatches the VGMs in response to a specified target trajectory. The NRMSE associated with the increased portion of the population devices not reporting state-information is shown in Figure 5.17.

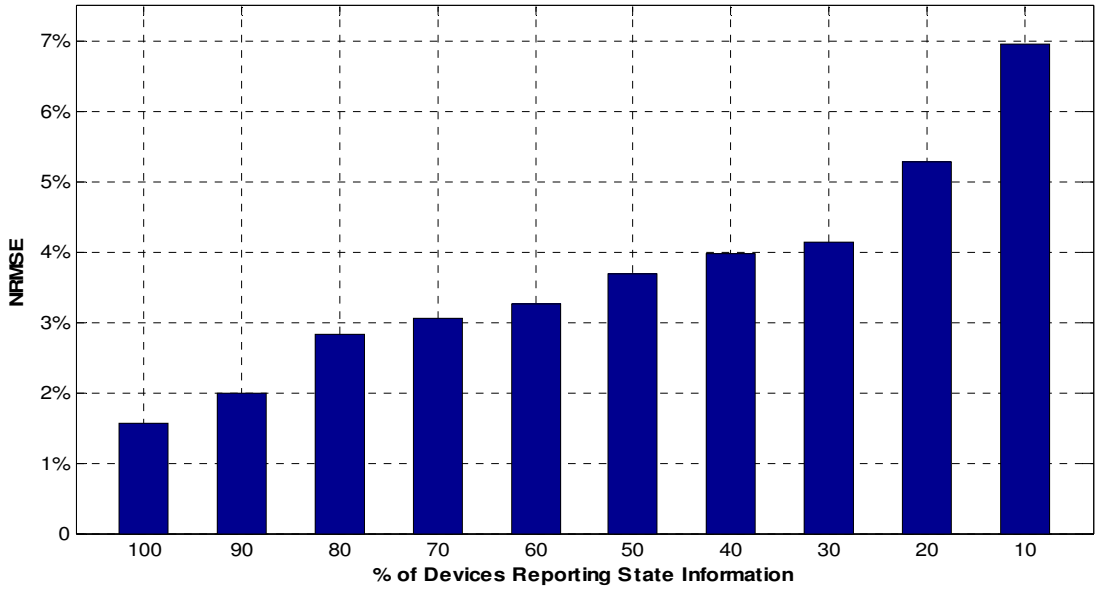

Figure 5.17- NRMSE for Different Levels of Device-State Reporting.

As shown in Figure 5.17, the error associated with the VGM response increases as device-state information is decreased, as would be expected. However, even at very low state-information levels the normalized root mean squared error associated with the demand response system remains below 8%. Once again, this error is largely attributed to discretization of the deadband region, and quantized device-level power ratings; although the reduced information scenarios amplifies these effects considerably. The response of the individual load communities, as well as their feasible regions, are shown in Figure 5.18 for the 100%, 80%, and 50% knowledge scenarios.

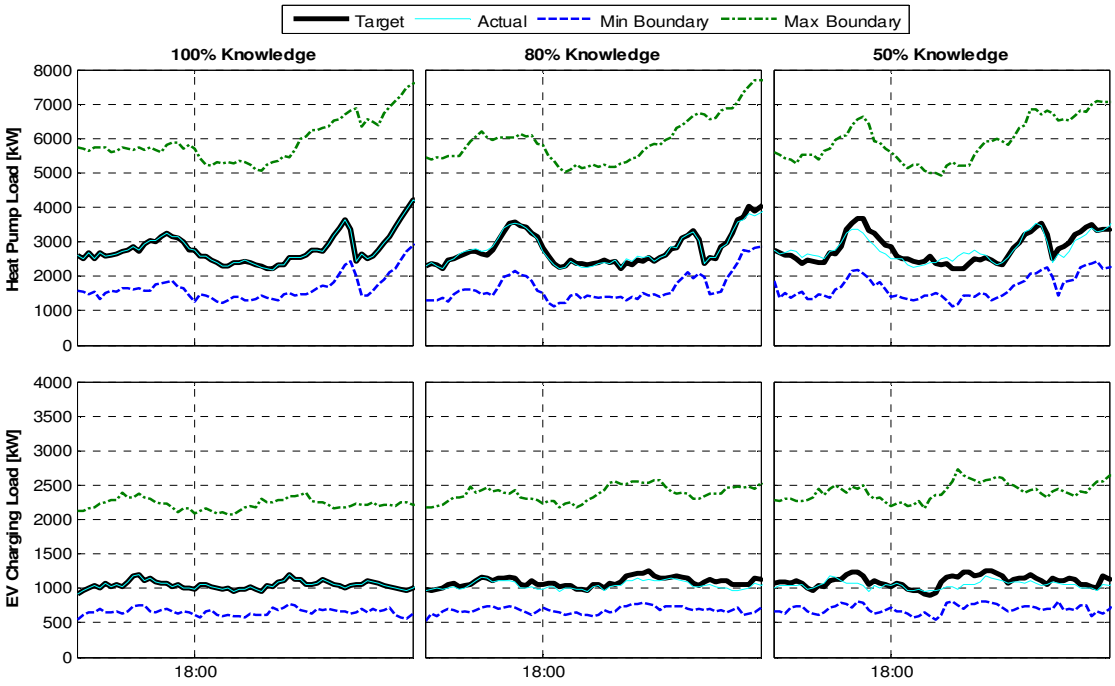

Figure 5.18 - Individual VGM response for 100%, 80%, and 50% knowledge scenarios.

It is apparent from Figure 5.18 that the heat pump VGM provides the most consistent response for all device-state knowledge scenarios, as the individual participating loads of the EV population are once again connecting and disconnecting from the system throughout the day. This additional uncertainty in the EV population results in greater error under limited knowledge scenarios, as shown in Figure 5.19.

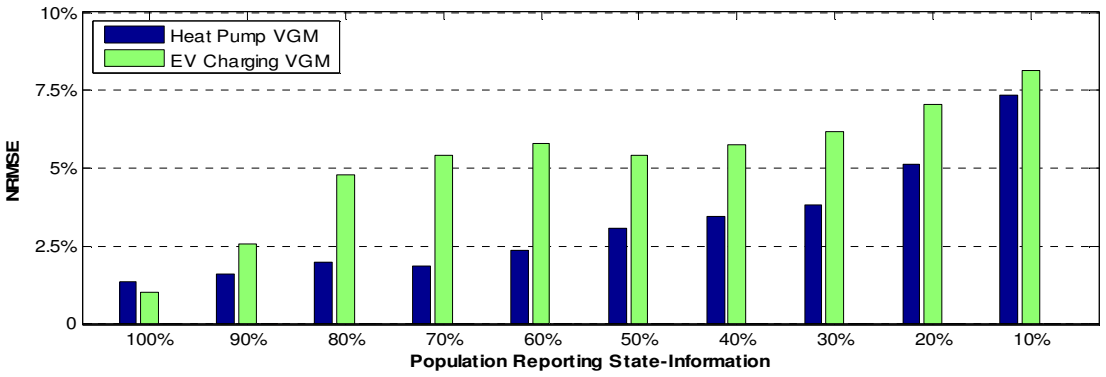

Figure 5.19 - NRMSE associated with individual VGM populations for various knowledge levels.

It is evident that the error associated with the EV Charging VGM increases more quickly than the error of the Heat Pump VGM. This is due to the dynamic population size of the

EV Charging VGM; As a result, the controller must estimate the number of devices in the population that are available and predict their device states, whereas the Heat Pump VGM must only estimate the device states as they are always connected to the load control system. Further system improvements could be realized by having EV charging stations indicate if a vehicle is currently drawing power from the grid, reducing the uncertainty for the EV Charging VGM. This would be particularly suitable for public charging stations, as it would provide no information regarding the individual user – only the presence or absence of any EV charging at the station.

Under moderate uncertainty scenarios, where the majority of devices are reporting device-state information, the resultant system error increases at a rate of approximately 1% for every 10% of devices not reporting state information. It is important to note, however, that the difference between full device-state knowledge and 90% device-state knowledge results in a significant increase in demand response system NRMSE of approximately 1.75%.

5.2.2 Capacity Determination for Ancillary Service Provision

Further simulations were conducted to determine the effects of population size on available capacity, total energy dispatched, and the control signal amplitude and variability of the demand response program. This is crucial information for utility systems operators as they must determine how many responsive loads to recruit to provide a required amount of capacity for ancillary services. In addition, this will provide utility operators with insight into the instrumentation requirements to establish a demand response program with their desired level of accuracy and capacity.

To achieve this, heterogeneous populations of equal numbers of heat pumps and EV charging loads were simulated, ranging from 500 devices up to 6000 devices per VGM. In each scenario the target trajectory was iteratively scaled to ensure that the demand response program could achieve the desired output throughout the entire simulation period. As expected, the energy dispatched by the demand response program scaled linearly with population size. This is due to the fact that the target trajectory was scaled linearly, and identical constraints were given to determine the magnitude of the target trajectory – specifically that the demand response program never be over-dispatched beyond feasible

target values. Figure 5.20 shows the energy dispatched by the DR program for various population sizes with 100% device-state information.

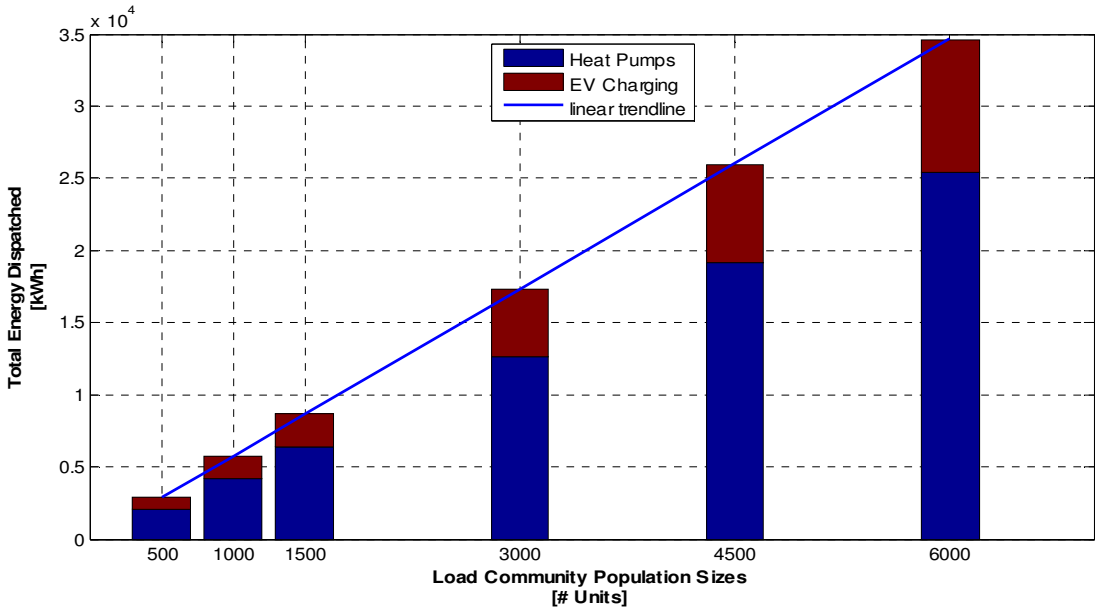

Figure 5.20 - Energy Dispatched vs Population Size for 100% Knowledge Scenarios.

Once feasible target trajectories had been established for the evaluated populations of devices participating in the DR program, additional simulations were conducted to evaluate the impacts of limited device-state knowledge. For each population size, simulations were conducted ranging from 100% device-state knowledge down to 50% device-state knowledge in 10% increments. The associated NRMSE for each device-state knowledge scenario is summarized in Figure 5.21.

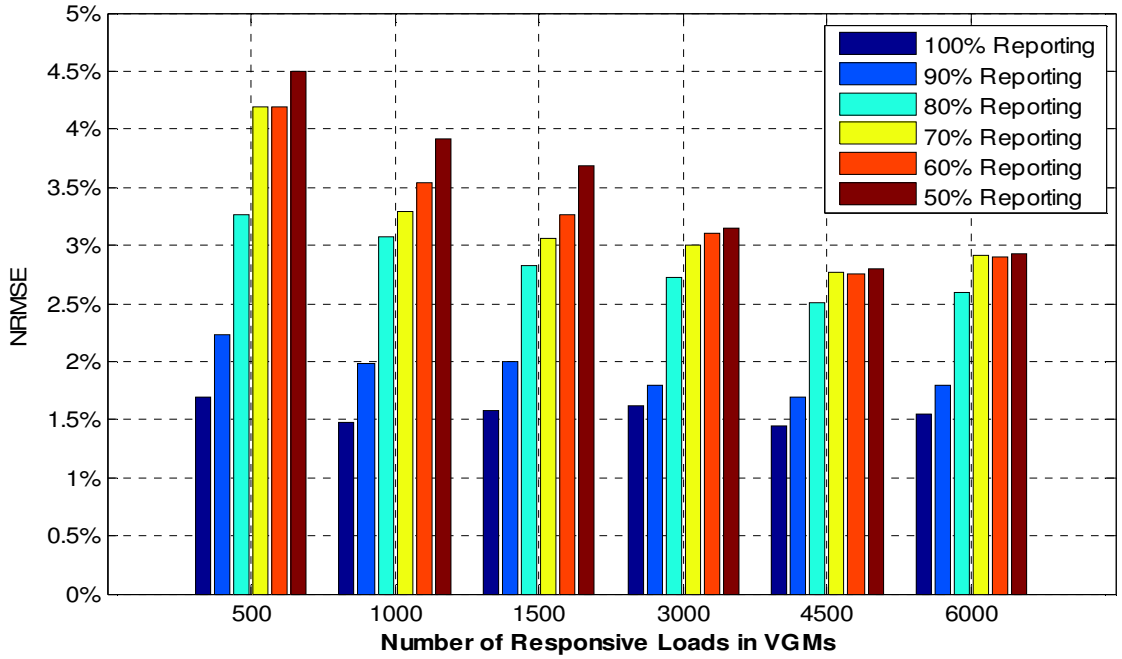

Figure 5.21 - NRMSE of Responsive Load Populations of Various Sizes under Limited Device-state Information Scenarios.

As shown in Figure 5.21, the error associated with the reduction in device-state knowledge follows the same trend as was established in Section 5.2.1, with a marked increase in error when departing from the 100% device-state knowledge scenario, but remaining less than 5% NRMSE even when device state-knowledge was limited to 50% of the responsive populations. However, the NRMSE associated with the demand response program began to increase slightly when population sizes reaches 6000 devices per VGM. These large populations result in a crowding of the discrete bins used by the controller when dispatching the VGMs, and as a result the increments between bins are larger and not as likely to match the target trajectory exactly. The use of more bins in the control algorithms, or splitting a larger population into two independent smaller VGMs could address this increased error. Figure 5.22 shows the mean available capacity, or flexibility, of the VGMs for the various population sizes investigated.

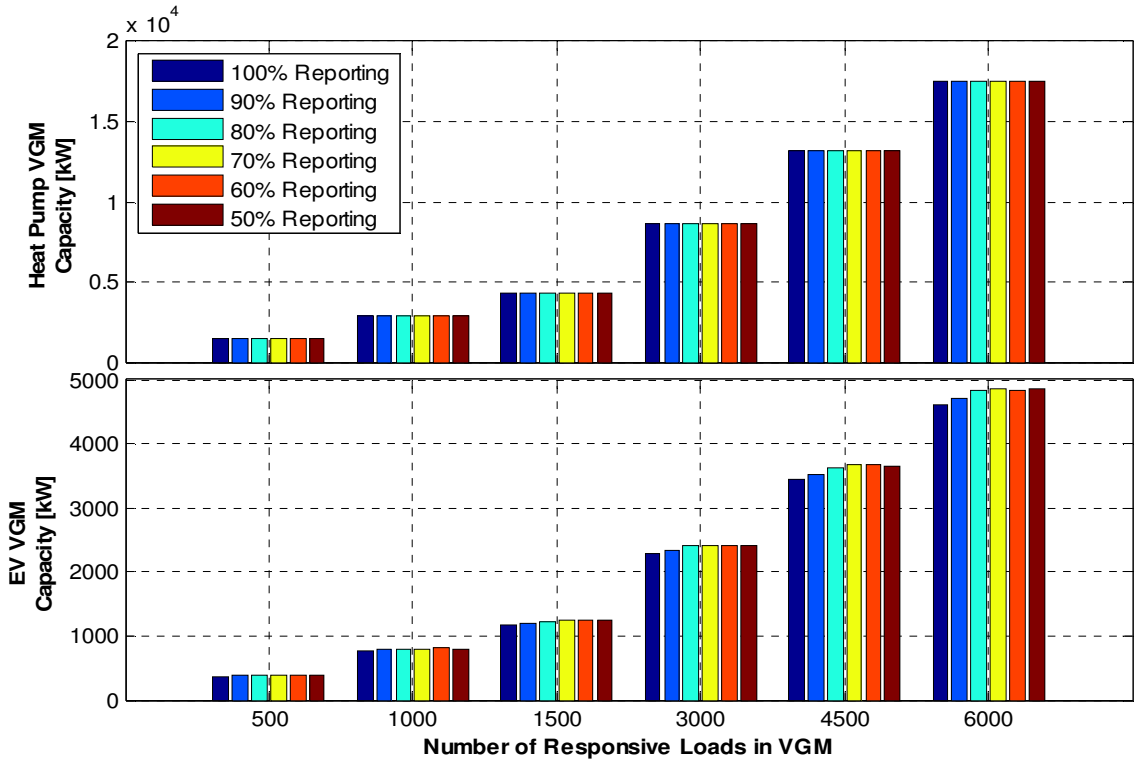

Figure 5.22 - Mean Available Capacity of VGMs vs Population Size.

The mean available capacity of the demand response program shows a linear correlation with population sizes, with slight overestimation of available capacity of the EV Charging VGMs in the reduced device-state knowledge scenarios for larger populations. Despite this overestimation of the available capacity, the demand response controller is able to provide ancillary services functionality with similar error levels for all population sizes investigated, with only minor increases in error for the largest populations tested. The primary cause of the increased capacity of the EV Charging VGM under reduced device-state knowledge scenarios is the requirement of the controller to estimate whether a vehicle is plugged into a charger or being used by a customer.

Finally, the disruptiveness of the demand response program on end-user functionality was investigated with respect to population size through the mean control signal magnitude and control signal standard deviation for each population size, as summarized in Figure 5.23.

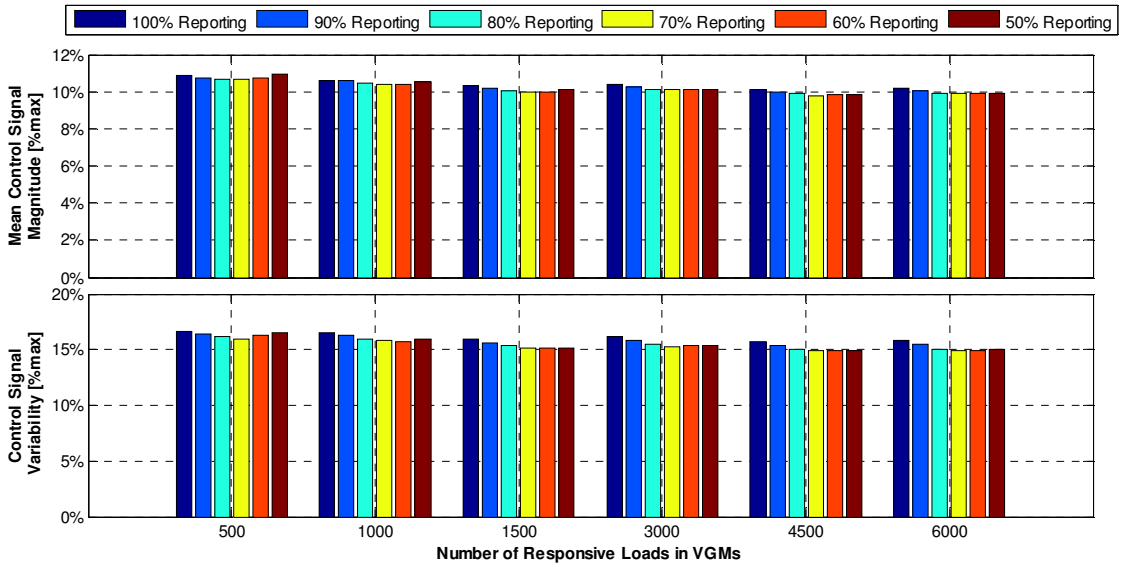

Figure 5.23 – Heat Pump VGM control signal magnitude and variability for various population sizes and device-state knowledge scenarios.

The magnitude and variability of the control signal do not change significantly with increases in population size for either VGM, both differing by less than 2% across all simulations conducted. There is a slight trend towards a reduction in control signal magnitude and variability as population size is increased, but this variation may be largely attributed to minor differences in the distribution of load power ratings among the populations.

Based on this analysis, it can be shown that as the number of participating loads increases the available capacity and energy dispatched by the demand response program will scale linearly if the target trajectory is scaled in the same manner. As population sizes reach 6000 devices per VGM, the associated NRMSE begins to increase slightly. Additionally, the increase in computational time required once populations of participating loads were increased beyond 6000 devices per VGM, indicates a potential limit on individual VGM population size. However, this could be alleviated by dividing larger populations of participating loads into multiple smaller VGMs, permitting distribution of computational requirements and concurrent calculations to be completed. This approach has the added benefit of allowing a utility operator to utilize individual VGMs for different services as required.

Another interesting observation from Figure 5.23 is that under the current target trajectory the VGMs are generally under-utilized for all but a few minutes of the simulation when the target reaches the feasible VGM boundary. While this serves to further minimize the inconvenience on end-user functionality of the participating loads, it is also inefficient for utility operators. It may be possible to achieve greater utilization with minimal impacts on end-user functionality by truncating the target trajectory signal to eliminate the large peaks in demand, effectively allowing the utility operators to request increased amounts of dispatched energy over the same operational period. This would, however, necessitate the operation of conventional generation resources, or additional DR programs, to meet the portion of the target trajectory that was truncated in the first place. Real-world experience in the operation of DR programs would provide utility operators with further opportunity to refine DR target determination to optimize the system utilization while ensuring end-use comfort constraints are not affected. Further, analysis of the system response under prolonged saturation of the VGMs must be investigated to ensure undesirable behavior is not inadvertently initiated.

6 Conclusions

6.1 Main Contributions

This thesis has examined the effectiveness of aggregate demand response programs utilizing residential scale loads under varying levels of device-state information. The development of a new simulation tool to model residential scale loads, as well as a demand response control framework to test various control algorithms, was created to facilitate the investigation. The simulation models thermostatically controlled heating loads of residential homes using an equivalent thermal parameter approach, and electric vehicle charging loads using a quasi-steady state formulation.

A number of control algorithms were implemented to determine the effectiveness of demand response programs, culminating in a series of case studies using demand response to provide ancillary services to power systems operators, and to smooth wind generation injections into the electrical grid. In addition, the model was adopted to allow the operation of the demand response program when a portion of the participating loads do not provide any device-state information to the centralized controller. From these case studies, it was found that:

- The model works for multiple target trajectories, population sizes and compositions, over any specified time period. When simulations with reduced device state-information were evaluated, only small increases in the response error were noted. Specifically, the NRMSE associated with the demand response program increases approximately 1% for every 10% decrease in device-state knowledge in the VGM populations. As a result, even for cases with a device-state knowledge of 50% of the populations, the associated NRMSE remains below 5%. This holds true for VGM population sizes ranging from 500 devices to 6000 devices. Further reductions of the NRMSE associated with reduced-knowledge DR scenarios could be achieved via additional error-correction algorithms integrated into the DR control algorithms.
- While both investigated loads (Home heat pumps and EV charging) were successfully implemented as VGMs, the home heat pump loads provided the

greatest degree of flexibility in all simulations. This is largely due to the fact that the heat pump loads are available and participating in the demand response program throughout the simulation period, while the EV charging loads are regularly entering and leaving the load community as they are driven by end-users. However, EV charging loads are not significantly affected by seasonal temperature variations, whereas the home heat pump loads become less effective as outdoor air temperatures approach the thermostat set point temperature. For this reason, EV charging loads exhibit the greatest year-round potential for utilization in demand response programs.

- The utilization of the demand response resource under the proposed target trajectories was very low – approximately 15% or less of the potential resource available over the simulation period. However, this was necessary to ensure that the highly variable target trajectories remained within the VGM feasible regions throughout the simulation. It may be possible to better utilize the demand response resources via optimization of the target trajectory, and optimal dispatch of demand response resources in conjunction with conventional generation resources.
- Short-duration target trajectories that call upon the full available capacity of the demand response population do not appear to produce any undesirable behavior from the system. Some device-level synchronization was observed when the target trajectory reached the feasible limits of the VGMs, however device-state diversity rapidly restored without any intervention from the controller when the peak trajectory was reduced. The effects of long-duration VGM maximum output were beyond the scope of this thesis.
- The available demand response resource scales proportionally with the population size of the participating VGMs. Doubling of the participating population of a particular load type results in a similar doubling of the available capacity and the energy dispatched by the DR program, provided a similarly scaled target trajectory is specified. This information will provide a valuable baseline to utility systems operators when considering how many loads to recruit for a demand response program.

- The error associated with VGMs decreases as the population size is increased to a certain point, however when the population size reaches 6000 loads per VGM the associated error begins to increase again. This effect is further amplified in the case of reduced device-state information scenarios. In addition, with population sizes of 6000 units and larger the associated computational time increases substantially.

The demand response algorithms and the modeling framework developed in this thesis should be useful in further studies of demand response programs, both at the control systems level to determine optimal control hardware for participating loads, quantifying the transient response from a demand response control program, and in large-scale planning of utility systems operation.

6.2 Recommendations for Future Work

Further development of appropriate algorithms for demand response programs of aggregate residential scale loads could be carried out in several areas. One key area of improvement is the implementation of a feedback mechanism to further reduce the error associated with reduced device-state information scenarios. A simple PID controller could be implemented to correct for differences between the anticipated response to a given control signal and the actual response of the system, and applying a gain factor to iteratively tune the controller for the next time-step.

Another opportunity for future work lies in establishing a rational and economic model to provide incentives for devices to participate in demand response programs and to quantify the benefits to the end-user for their participation.

The individual device models used in the simulations provide adequate fidelity for evaluating the aggregate demand response of the system, but the EV charging model could be updated to better account for device-level charging phenomenon that are beyond the scope of the quasi semi-state framework used in this thesis. In addition, inclusion of vehicle-to-grid functionality would provide insight into the potential of EV charging loads to provide demand response services beyond what is possible with only deferred charging. Further, an investigation into the effects of the battery charging trajectory specified by the demand response program on battery performance and health is necessary prior to implementation of such a system on actual EVs.

As the specified target trajectories in this thesis resulted in low utilization of the demand response resources, further research into optimal target trajectory formulation would provide significant value to utility systems operators. This could be completed in conjunction with work to reduce the computational complexity of the control algorithms for large population VGMs, as well as large-scale implementations of the simulations to include multiple VGMs of similar load types. In addition to improving the utilization of the demand response resource, this would enable to evaluation of much larger DR programs by recruiting many loads into multiple VGMs, eliminating the associated increased error and computational requirements of large population VGMs. Furthermore, it is necessary to investigate the effects of a controller requesting the maximum (or minimum) feasible output from a VGM for a prolonged period of time. It may be possible to drive the system to saturation if maximum output is requested for a sufficiently long time, and a recovery period may be required prior to the VGM being available to provide DR services immediately following such a request.

Finally, development of consumer-friendly hardware to enable demand response participation of residential scale loads, and the underlying control structure of such devices is necessary to bring the simulated demand response programs into the real-world environment. A discrete control algorithm, similar to the one used by Chassin [20], may be necessary to fully characterize the control system transfer function and transient response of the DR system.

7 References

[1] BC Hydro, “Integrated Resource Plan November 2013,” BC Hydro, Vancouver, BC, Canada, 2013.

[2] W. Miao, H. Jia, D. Wang, S. Parkinson, C. Crawford, and N. Djilali, “Active Power Regulation of wind power systems through demand response,” Science China Technological Series, Vol. 55, No. 6: 1667-1676, June 2012.

[3] S. Parkinson, D. Wang, N. Djilali, “Toward Low Carbon Energy Systems: The Convergence of Wind Power, Demand Response, and the Electricity Grid.” IEEE PES Innovative Smart Grid Technologies, 2012.

[4] BC Hydro, “Electric Load Forecast Fiscal 2013 to Fiscal 2033” BC Hydro, Vancouver, BC, Canada, 2012.

[5] California Independent System Operator, “Demand Response & Proxy Demand Resource – Frequently Asked Questions 6/24/2011,” CAISO, Folsom, CA, USA, 2011. [Online]. Available: http://www.caiso.com/Documents/DemandResponseandProxyDemandResourcesFrequentlyAskedQuestions.pdf

[6] D. Letto and R. George, “Examination of the Potential for Industrial Loads to Provide Ancillary Services” ENBALA Power Networks for Oak Ridge National Laboratory under Subcontract#: 4000114170, November 2012.

[7] Parkinson, Simon, "Managing Sustainable Demand-side Infrastructure for Power System Ancillary Services", *M.A.Sc. Thesis*, University of Victoria, December 2011.

[8] J. Matheiu, S. Koch, and D. Callaway, “State Estimation and Control of Electric Loads to Manage Real-Time Energy Imbalance” IEEE Transactions on power systems, vol 28. No 1. February 2013.

[9] D. Li, Z. Aung, J. Williams, and A. Sanchez, “No peeking: privacy-preserving demand response system in smart grids,” International Journal of Parallel, Emergent and Distributed Systems, Vol. 29, No. 3, 290-315, 2014.

[10] T. Williams, D. Wang, C. Crawford, and N. Djilali, “Integrating renewable energy using a smart distribution system: Potential of self-regulating demand response,” Renewable Energy 52 46-56 (2013).

[11] Canadian Electricity Association, “Power Generation in Canada: A Guide,” Canadian Electricity Association, Ottawa, ON, Canada, 2006.

[12] G. Cornelis van Kooten. Wind power: the economic impact of intermittency. *Letters in Spatial and Resource Sciences,* 3(1):1-17, 1990.

[13] US Energy Information Administration, “Updated Capital Cost Estimates for Utility Scale Electricity Generating Plants,” US Department of Energy, Washington, DC, USA 2013 [Online] Available: http://www.eia.gov/forecasts/capitalcost/pdf/updated_capcost.pdf

[14] E. Yearwood-Lee, “The Site C Dam: Historic Overview and Key Issues,” Legislative Library of British Columbia, Victoria, BC, Canada, 2007.

[15] J. McLean, “Canada’s Nuclear Energy Sector: Where to from Here?” Canada’s Public Policy Forum, Ottawa, ON, Canada, January 2014. [Online] Available: http://site.ebrary.com.ezproxy.library.uvic.ca/lib/uvic/reader.action?docID=10830870

[16] United States Geological Survey, “Hydroelectric power water use,” USGS, US Department of the Interior, USA, 2014 [Online] Available: http://water.usgs.gov/edu/wuhy.html

[17] BC Hydro, “Site C Clean Energy Project: Business Case Summary,” BC Hydro, Vancouver, BC, Canada, 2014.

[18] G. St. Denis and P. Parker, “Community energy planning in Canada: The role of renewable energy,” Renewable and Sustainable Energy Reviews 13 (2009).

[19] Bonneville Power Authority, “BPA Balancing Reserves Deployed,” BPA, USA, 2015. [Online] Available: http://transmission.bpa.gov/business/operations/wind/reserves.aspx

[20] Chassin, David, "New Residential Thermostat for Transactive Systems", *M.A.Sc. Thesis*, University of Victoria, December 2014.

[21] R.G. Pratt, P.J. Balducci, C. Gerkensmeyer, S. Katipamula, M.C.W. KintnerMeyer, T.F. Sanquist, K.P. Schneider, and T.J. Secrest. The smart grid: An estimation of the energy and CO2 benefits. Technical Report 19112 Revision 1, Pacific Northwest National Laboratory, Richland, Washington, January 2010.

[22] M. Madrigal and K Porter, "Operating and Planning Electricity Grids with Variable Renewable Generation," The World Bank, Washington, DC, USA, 2013.

[23] J. Apt and P Jaramillo, "Variable Renewable Energy and the Electricity Grid," RFF Press, New York, NY, USA, 2014.

[24] A. Jain and K. Garg, "Variable Renewable Generation and Grid Operation," 2010 International Conference on Power System Technology, 2010.

[25] S. Sundararagavan and E. Baker. Evaluating energy storage technologies for wind power integration. *Solar Energy 86 (2012).*

[26] A. Tuohy, H. Kamath, and L. Rogers, "Evaluation of Storage for Bulk System Integration of Variable Generation," 2012 IEEE Power and Energy Society General Meeting, 2012.

[27] G. Carpinelli, G. Celli, S. Mocci, F. Mottola, F. Pilo, and D. Proto, "Optimal Integration of Distributed Energy Storage Devices in Smart Grids," IEEE Transactions on smart grid, Vol. 4, No, 2, June 2013.

[28] S. Gill, E. Barbour, I. Wilson, and D. Infield, "Maximising revenue for non-firm distributed wind generation with energy storage in an active management system," IET Renewable Power Generation, 2013.

[29] N. O'Connell, P. Pinson, H. Madsen, and M. O'Malley, "Benefits and Challenges of Electrical Demand Response: A Critical Review. *Renewable and Sustainable Energy Reviews 39* (2014)

[30] P. Faria, Z. Vale, "Demand response in electrical energy supply: An optimal real time pricing approach," Energy 36 (2011).

[31] D. Chassin, D. Hammerstrom, and J. DeSteese, "The Pacific Northwest Demand Response Market Demonstration," 2008 IEEE Power and Energy Society General Meeting - Conversion and Delivery of Electrical Energy in the 21st Century.

[32] S. Widergren, K. Subbarao, D. Chassin, J. Fuller, and R. Pratt, "Residential Real-time Price Response Simulation," 2011 IEEE Power and Energy Society General Meeting.

[33] S. Gyamfi, S. Krumdieck, and T. Urmee, "Residential peak electricity demand response – Highlights of some behavioural issues," Renewable and Sustainable Energy Reviews 25 (2013).

[34] Johanna L. Mathieu. "Modeling, Analysis, and Control of Demand Response Resources." *PhD dissertation*, University of California, Berkley, Spring 2012

[35] D. Wight, et al, "2010 Assessment of Demand Response and Advanced Metering Staff Report," Federal Energy Regulatory Commission, USA, 2011.

[36] PJM, "The Evolution of Demand Response in the PJM Wholesale Market," PJM Interconnection, October 2014.

[37] D. Hess and J. Coley, "Wireless smart meters and public acceptance: The environment, limited choices, and precautionary politics," Public Understanding of Science Vol. 23 No. 6: 688-702. 2014.

[38] Marbek Resource Consultants Ltd. BC Hydro 2007 Conservation Potential Review. Technical report, Prepared for BC Hydro, 2007.

[39] NRC OEE. 2007 Survey of Household Energy Use: Detailed Statistical Report. Technical report, Natural Resources Canada Office of Energy Efficiency, 2007.

[40] F.Oldewurtel, et al. "A Framework for and Assessment of Demand Response and Energy Storage in Power Systems" in *2013 IREP Symposium-Bulk Power System Dynamics and Control*, 2013.

[41] W. Kempton, et al. "A test of vehicle-to-grid (V2G) for energy storage and frequency regulation in the PJM system." Technical report, Mid-Atlantic Grid Interactive Cars Consortium, 2009.

[42] C. Quinn, D. Zimmerle, and T.H. Bradley. The effect of communication architecture on the availability, reliability, and economics of plug-in hybrid electric vehicle-to-grid ancillary services. J. of Power Sources, 195(5):1500–1509, 2010.

[43] L. Melbourne, "National Travel Survey: England 2013," Department for Transport, London, UK, 2013.

[44] R. Mortensen and K. Haggerty. A stochastic computer model for heating and cooling loads. IEEE Trans. Power Syst., 3(3):854–860, 1990.

[45] D.S. Callaway and I. Hiskens. Achieving controllability of electric loads. Proc. of IEEE, 99(1):184–199, 2011.

[46] Y. Sun, M. Elizondo, S. Lu, and J. Fuller, "The Impact of Uncertain Physical Parameters on HVAC Demand Response," IEEE Transactions on Smart Grid, Vol. 5, no. 2, March 2014.

[47] D. Wang, S. Parkinson, W. Miao, H. Jia, C. Crawford, and N. Djilali, "Online voltage security assessment considering comfort-constrained demand response control of distributed heat pump systems," Applied Energy 96 (2012).

[48] H. Madsen and J. Holst. Estimation of continuous-time models for the heat dynamics of a building. Energy and Buildings, 22(1):67–79, 1995.

[49] J. Sager, "Cold Climate Air Source Heat Pumps," Canmet Energy, National Resources Canada, 2013. [Online] Available: http://www.chba.ca/uploads/TRC/May%202013/Cold%20Climate%20Air%20Source%20Heat%20Pumps%20Presentation%20-%20May%202013.pdf

[50] PNNL. GridLabD - Power System Simulation Software. U.S. Department of Energy: Pacific Northwest National Laboratory http://www.gridlabd.org/, 2011.

[51] D.S. Callaway. "Tapping the energy storage potential in electric loads to deliver load following and regulation, with application to wind energy," Energy Conversion and Management, 50(9):1389–1400, 2009.

[52] John Axsen, et al. “The Canadian Plug-in Electric Vehicle Survey (CPEVS 2013): Anticipating Purchase, Use, and Grid Interactions in British Columbia.” Simon Fraser University, Vancouver, BC, Tech. Rep. October, 2013.

[53] J.F. Manwell, J.G. McGowan, and A.L. Rogers. Wind Energy Explained: Theory, Design and Application, 2nd Edition. John Wiley and Sons, 2010.

[54] C.G. Justus. Winds and Wind System Performance. Franklin Institute Press, Philadelphia PA, 1978.

[55] J. Cotrell. A preliminary evaluation of a multiple-generator drivetrain configuration for wind turbines. In Proc. of 21st ASME Wind Energy Symposium, pages 345–352, 2002.

[56] National Renewable Energy Laboratory (Sept 2014). National Wind Technology Center M2 Tower Data. [Online]. Available: http://www.nrel.gov/midc/nwtc_m2/

[57] Hoevenaars, Eric, "Temporal Resolution in Time Series and Probabilistic Models of Renewable Power Systems", *M.A.Sc. Thesis*, University of Victoria, April 2012.

[58] L. Kelly. “Probabilistic modelling of plug-in hybrid electric vehicle: Impacts on distribution networks in British Columbia.” M.A.Sc. Thesis: University of Victoria Department of Mechanical Engineering, 2010.

[59] Foley, Aoife M., et al. “Current methods and advances in forecasting of wind power generation” Renewable Energy 37 (2012)